

# Inclusive Charged–Current Neutrino–Nucleus Reactions

J. Nieves,<sup>1</sup> I. Ruiz Simo,<sup>2</sup> and M. J. Vicente Vacas<sup>2</sup>

<sup>1</sup>*Instituto de Física Corpuscular (IFIC), Centro Mixto Universidad de Valencia-CSIC,  
Institutos de Investigación de Paterna, E-46071 Valencia, Spain*

<sup>2</sup>*Departamento de Física Teórica and IFIC, Centro Mixto Universidad de Valencia-CSIC,  
Institutos de Investigación de Paterna, E-46071 Valencia, Spain*

We present a model for weak CC induced nuclear reactions at energies of interest for current and future neutrino oscillation experiments. This model is a natural extension of the work of Refs. [1, 2], where the QE contribution to the inclusive electron and neutrino scattering on nuclei was analyzed. The model is based on a systematic many body expansion of the gauge boson absorption modes that includes one, two and even three body mechanisms, as well as the excitation of  $\Delta$  isobars. The whole scheme has no free parameters, besides those previously adjusted to the weak pion production off the nucleon cross sections in the deuteron, since all nuclear effects were set up in previous studies of photon, electron and pion interactions with nuclei. We have discussed at length the recent charged current quasi-elastic MiniBooNE cross section data, and showed that two nucleon knockout mechanisms are essential to describe these measurements.

PACS numbers: 25.30.Pt, 13.15.+g, 24.10.Cn, 21.60.Jz

## I. INTRODUCTION

The interaction of neutrinos with nuclei at intermediate energies plays an important role in the precise determination of neutrino properties such as their masses and mixing parameters. It can also provide relevant information on the axial hadronic currents. The statistical significance of the experiments is rapidly improving. However, the data analysis needs to consider a large number of nuclear effects that distort the signals and produce new sources of background that are absent in the elementary neutrino nucleon processes.

In this context, it is clearly of interest the elaboration of a theoretically well founded and unified framework in which the electroweak interactions with nuclei could be systematically studied. Furthermore, the recent measurements of the cross sections for several channels [3–6] provide a serious benchmark to the theoretical models. An excellent review of the current situation can be found in Ref. [7].

A suitable theoretical model should include, at least, three kinds of contributions: (i) quasielastic (QE) for low energy transfers, (ii) pion production and two-body processes from the QE region to that around the  $\Delta(1232)$  resonance peak, and (iii) double pion production and higher nucleon resonance degrees of freedom induced processes at even higher energies. A word of caution is needed here, because the same words could refer to somehow different magnitudes in the literature. For instance, whereas in most theoretical works QE is used for processes where the gauge boson  $W^\pm$  or  $Z^0$  is absorbed by just one nucleon, which together with a lepton is emitted<sup>1</sup>, in the recent MiniBooNE papers, QE is related to processes in which only a muon is detected. This latter definition could make sense because ejected nucleons are not detected in that experiment, but includes multinucleon processes and others like pion production followed by absorption. However, it discards pions coming off the nucleus, since they will give rise to additional leptons after their decay. In any case, their experimental results cannot be directly compared to most previous calculations.

The QE processes have been abundantly studied. Simple approaches using a global Fermi gas for the nucleons and the impulse approximation are good enough to describe qualitatively electron scattering but more sophisticated treatments of the nuclear effects are necessary to get a detailed agreement with data. There are different kinds of models like those based on the use of proper nucleon spectral functions [8–10], others in which nucleons are treated in a relativistic mean field [11, 12] and models based on a local Fermi gas including many body effects such as spectral functions [13] and RPA [2, 14–16]. Concerning the elementary process,  $\nu + N \rightarrow l + N'$ , the hadronic vector current is well known from electron scattering. The axial current, after the use of the partial conservation of the axial current to relate the two form factors and assuming a dipole form, depends on two parameters:  $g_A$ , that can be fixed from the neutron  $\beta$  decay and the axial mass  $M_A$ . The value of  $M_A$  established from QE data on deuterium targets is

---

<sup>1</sup> This follows the traditional nomenclature of electronuclear scattering. Note that in some cases the resulting nucleon after the absorption of the gauge boson is not emitted, but rather it could be trapped and form part of a bound state of the daughter nucleus (discrete transition).

$M_A = 1.016 \pm 0.026$  [17] GeV. A consistent result is obtained from  $\pi$  electro-production after chiral corrections are incorporated [18, 19].

The predicted cross sections for QE scattering are very similar for most models. See, e.g., the compilation shown in Fig. 2 of Ref. [20]. On the other hand, the theoretical results are clearly below the recently published MiniBooNE data [3]. The discrepancy is large enough to provoke much debate and theoretical attention. Some works try to understand these new data in terms of a larger value of  $M_A$ . For instance, in Ref. [3] a value of  $M_A = 1.35 \pm 0.17$ , that also fits the  $Q^2$  shape, is suggested. Consistent values are obtained in Refs. [21–23]. This idea is not only difficult to understand theoretically, but is also in conflict with higher energy NOMAD data [24] ( $M_A = 1.06 \pm 0.02(stat) \pm 0.06(syst)$  GeV). In another line of research, the role of meson exchange currents [25] and superscaling [26] have been also estimated recently. Finally, another idea has been explored in Refs. [27, 28], which include two nucleon mechanisms (and others related to  $\Delta$  excitation) and reproduce MiniBooNE QE data without the need of a large value of  $M_A$ . These latter results suggest that much of the experimental cross section can be attributed to processes that are not properly QE, stressing again the need of a unified framework dealing with all relevant mechanisms, namely  $\pi$  production and multinucleon excitation.

The matter of  $\pi$  production induced by neutrinos is also of much interest [29–36]. The elementary reaction on the nucleon, at low and intermediate energies, includes both background and resonant mechanisms. The background terms can be obtained from the chiral lagrangians. The resonant terms contain some free parameters that have been adjusted to ANL and/or BNL old bubble chamber data. Still, the experimental data have large normalization uncertainties which are certainly reflected in the theoretical models. At low energies, the  $\Delta(1232)$  resonance plays a very important role in this process, and for small  $Q^2$  values only one form factor ( $C_5^A$ ) is relevant. Thus, special attention has been addressed to its study with recent results ranging from  $C_5^A(0) = 1.19 \pm 0.08$  [31], obtained neglecting the non resonant background, to  $C_5^A(0) = 1.00 \pm 0.11$  [35] in a more complete model. This latter value implies a 20% reduction with respect to the off-diagonal Goldberger-Treiman relation (GTR). In nuclei, several effects are expected to be important for the  $\pi$  production reaction. First, the elementary process is modified by Fermi motion, by Pauli blocking and more importantly by the changes of the spectral function of the  $\Delta$  resonance in the medium. In addition, the final pion can be absorbed or scattered by one or more nucleons. This latter kind of effects do not modify the inclusive neutrino nucleus cross section and thus are out of the scope of this paper.

Our aim in this work is to extend the model of Ref. [2], which studied QE scattering. We will include two nucleon processes and  $\pi$  production in a well established framework that has been tested, for instance, in electron and photon scattering [1, 37]. This will extend the range of applicability of the model to higher transferred energies (and thus higher neutrino energies) and allow for the comparison with inclusive data which include the QE peak, the  $\Delta$  resonance peak and also the dip region between them. The structure of the paper is as follows: In Sect. II, we start establishing the formalism and reviewing briefly the approach for QE scattering of Ref. [2]. Then, we consider pion production mechanisms and two nucleon processes. Next, we discuss with special care the role of the  $\Delta$  resonance and how it is affected by the nuclear medium. In Sect. III we present and discuss some of the results derived from the model, and compare these to the recent MiniBooNE charged current (CC) QE and SciBooNE total cross section data. Finally in Sect. IV, we draw the main conclusions of this work.

## II. CC NEUTRINO/ANTINEUTRINO INCLUSIVE NUCLEAR REACTIONS

### A. General considerations

We will focus on the inclusive nuclear reaction

$$\nu_l(k) + A_Z \rightarrow l^-(k') + X \quad (1)$$

driven by the electroweak CC. The generalization of the obtained expressions to antineutrino induced reactions is straightforward (see Subsect. IIF). The double differential cross section, with respect to the outgoing lepton kinematical variables, for the process of Eq. (1) is given in the Laboratory (LAB) frame by

$$\frac{d^2\sigma_{\nu l}}{d\Omega(\hat{k}')dE'_l} = \frac{|\vec{k}'|}{|\vec{k}|} \frac{G^2}{4\pi^2} L_{\mu\sigma} W^{\mu\sigma} \quad (2)$$

with  $\vec{k}$  and  $\vec{k}'$  the LAB lepton momenta,  $E'_l = (\vec{k}'^2 + m_l^2)^{1/2}$  and  $m_l$  the energy and the mass of the outgoing lepton,  $G = 1.1664 \times 10^{-11}$  MeV<sup>-2</sup>, the Fermi constant and  $L$  and  $W$  the leptonic and hadronic tensors, respectively. To obtain Eq. (2) we have neglected the four-momentum carried out by the intermediate  $W$ -boson with respect to its mass, and have used the relation between the gauge weak coupling constant,  $g = e/\sin\theta_W$ , and the Fermi constant:

$G/\sqrt{2} = g^2/8M_W^2$ , with  $e$  the electron charge,  $\theta_W$  the Weinberg angle and  $M_W$  the  $W$ -boson mass. The leptonic tensor is given by<sup>2</sup>:

$$L_{\mu\sigma} = L_{\mu\sigma}^s + iL_{\mu\sigma}^a = k'_\mu k_\sigma + k'_\sigma k_\mu - g_{\mu\sigma} k \cdot k' + i\epsilon_{\mu\sigma\alpha\beta} k'^\alpha k^\beta. \quad (3)$$

The hadronic tensor corresponds to the charged electroweak transitions of the target nucleus,  $i$ , to all possible final states. It is given by<sup>3</sup>

$$W^{\mu\sigma} = \frac{1}{2M_i} \overline{\sum}_f (2\pi)^3 \delta^4(P_f - P - q) \langle f | j_{cc}^\mu(0) | i \rangle \langle f | j_{cc}^\sigma(0) | i \rangle^* \quad (4)$$

with  $P$  the four-momentum of the initial nucleus,  $M_i = \sqrt{P^2}$  the target nucleus mass,  $P_f$  the total four momentum of the hadronic state  $f$  and  $q = k - k'$  the four momentum transferred to the nucleus. The bar over the sum denotes the average over initial spins. The hadronic CC is given by

$$j_{cc}^\mu = \overline{\Psi}_u \gamma^\mu (1 - \gamma_5) (\cos \theta_C \Psi_d + \sin \theta_C \Psi_s) \quad (5)$$

with  $\Psi_u$ ,  $\Psi_d$  and  $\Psi_s$  quark fields, and  $\theta_C$  the Cabibbo angle. By construction, the hadronic tensor accomplishes

$$W^{\mu\sigma} = W_s^{\mu\sigma} + iW_a^{\mu\sigma} \quad (6)$$

with  $W_s^{\mu\sigma}$  ( $W_a^{\mu\sigma}$ ) real symmetric (antisymmetric) tensors. The hadronic tensor is determined by the  $W^+$ -boson selfenergy,  $\Pi_W^{\mu\sigma}(q)$ , in the nuclear medium. We follow here the formalism of Ref. [2], where it is shown that within the local density approximation, the hadronic tensor can be written as

$$W_s^{\mu\sigma} = -\Theta(q^0) \left( \frac{2\sqrt{2}}{g} \right)^2 \int \frac{d^3r}{2\pi} \text{Im} [\Pi_W^{\mu\sigma} + \Pi_W^{\sigma\mu}] (q; \rho) \quad (7)$$

$$W_a^{\mu\sigma} = -\Theta(q^0) \left( \frac{2\sqrt{2}}{g} \right)^2 \int \frac{d^3r}{2\pi} \text{Re} [\Pi_W^{\mu\sigma} - \Pi_W^{\sigma\mu}] (q; \rho). \quad (8)$$

Then, the differential cross section for the reaction in Eq. (1) is given by

$$\begin{aligned} \frac{d^2\sigma_{\nu l}}{d\Omega(\vec{k}') dk'^0} &= -\frac{|\vec{k}'|}{|\vec{k}|} \frac{G^2}{2\pi^2} \left( \frac{2\sqrt{2}}{g} \right)^2 \int \frac{d^3r}{2\pi} \text{Im} [L_{\mu\eta} \Pi_W^{\eta\mu}(q; \rho)] \Theta(q^0) \\ &= -\frac{|\vec{k}'|}{|\vec{k}|} \frac{G^2}{4\pi^2} \left( \frac{2\sqrt{2}}{g} \right)^2 \int \frac{d^3r}{2\pi} \left\{ L_{\mu\eta}^s \text{Im} [\Pi_W^{\mu\eta} + \Pi_W^{\eta\mu}] - L_{\mu\eta}^a \text{Re} [\Pi_W^{\mu\eta} - \Pi_W^{\eta\mu}] \right\} \Theta(q^0) \end{aligned} \quad (9)$$

with  $\Theta(\dots)$  the Heaviside step function.

The in medium gauge boson ( $W^\pm$ ) selfenergy depends on the nuclear density  $\rho(r)$ . We propose a many body expansion for  $\Pi_W^{\mu\sigma}$ , where the relevant gauge boson absorption modes would be systematically incorporated: absorption by one nucleon, or a pair of nucleons or even three nucleon mechanisms, real and virtual meson ( $\pi$ ,  $\rho$ ,  $\dots$ ) production, excitation of  $\Delta$  or higher resonance degrees of freedom, etc. In addition, nuclear effects such as RPA or Short Range Correlations (SRC) will be also taken into account. Some of the basic  $W$ -absorption modes are depicted in Fig. 1.

## B. Quasielastic scattering

The virtual  $W^+$  can be absorbed by one nucleon leading to the QE contribution of the nuclear response function. Such a process corresponds to a one particle-one hole (1p1h) nuclear excitation (first of the diagrams depicted in Fig. 1). This contribution was studied in detail in Ref. [2]<sup>4</sup>. Here, we will just briefly discuss the main features of the model. In Ref. [2], starting from a Local Fermi Gas (LFG) picture of the nucleus, which automatically accounts for Pauli blocking and Fermi motion, several nuclear corrections were incorporated, among others:

<sup>2</sup> We take  $\epsilon_{0123} = +1$  and the metric  $g^{\mu\nu} = (+, -, -, -)$ .

<sup>3</sup> In Eq. (4) the states are normalized such that  $\langle \vec{p} | \vec{p}' \rangle = (2\pi)^3 2p_0 \delta^3(\vec{p} - \vec{p}')$  and the sum over final states  $f$  includes an integration  $\int \frac{d^3p_j}{(2\pi)^3 2E_j}$ , for each particle  $j$  making up the system  $f$ , as well as a sum over all spins involved.

<sup>4</sup> The extension of this scheme for Neutral Currents (NC) was discussed in Ref. [14].

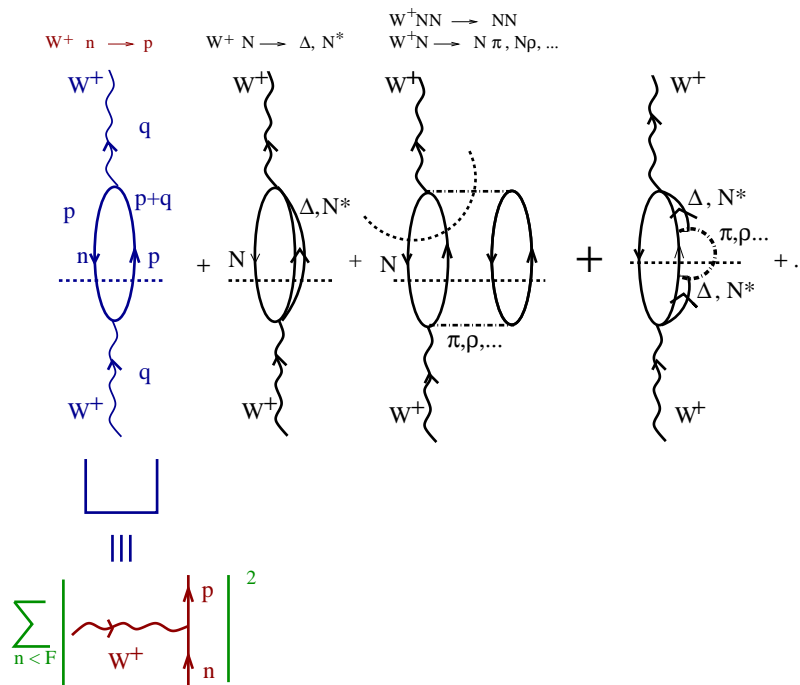


FIG. 1: Diagrammatic representation of some mechanisms contributing to the  $W^+$ -selfenergy.

- A correct energy balance, using the experimental  $Q$ -values, was enforced.
- Coulomb distortion of the charged leptons, important at low energies, was implemented by using the so called “modified effective momentum approximation”.
- Medium polarization (RPA), including  $\Delta$ -hole degrees of freedom and explicit pion and rho exchanges in the vector-isovector channel of the effective nucleon-nucleon force, and SRC effects were computed.
- The nucleon propagators were dressed in the nuclear medium, which amounts to work with nucleon spectral functions (a LFG of interacting nucleons) and it also accounts for some reaction mechanisms where the gauge boson is absorbed by two nucleons.

This model is a natural extension of previous studies on electron [1], photon [37] and pion [38–42] dynamics in nuclei. Even though the scarce existing CC data involve very low nuclear excitation energies, for which specific details of the nuclear structure might play an important role, the model of Ref. [2] provides one of the best existing combined descriptions of the inclusive muon capture in  $^{12}\text{C}$  and of the  $^{12}\text{C}(\nu_\mu, \mu^-)X$  and  $^{12}\text{C}(\nu_e, e^-)X$  reactions near threshold. Inclusive muon capture from other nuclei is also successfully described.

The theoretical errors affecting the predictions of Ref. [2] were discussed in Ref. [43]. There, it is concluded that is found to assume errors of about 10-15% on the QE neutrino-nucleus (differential and integrated) cross section results of Ref. [2].

The LFG description of the nucleus has been shown to be well suited for inclusive processes and nuclear excitation energies of around 100 MeV or higher [1, 37–42]. The reason is that in these circumstances one should sum up over several nuclear configurations, both in the discrete and in the continuum. This inclusive sum is almost insensitive to the details of the nuclear wave function<sup>5</sup>, in sharp contrast to what happens in the case of exclusive processes where

<sup>5</sup> The results of Ref. [2] for the inclusive muon capture in nuclei through the whole periodic table, where the capture widths vary from about  $4 \times 10^4 \text{ s}^{-1}$  in  $^{12}\text{C}$  to  $1300 \times 10^4 \text{ s}^{-1}$  in  $^{208}\text{Pb}$ , and of the LSND measurements of the  $^{12}\text{C}(\nu_\mu, \mu^-)X$  and  $^{12}\text{C}(\nu_e, e^-)X$  reactions near threshold indicate that the predictions of our scheme, for totally integrated inclusive observables, could be extended to much smaller, ( $\approx 10$  or  $20$  MeV), nuclear excitation energies. In this respect, Refs. [44] and [45] for inclusive muon capture and radiative pion capture in nuclei, respectively, are enlightening. In these works, continuum shell model and LFG model results are compared for several nuclei from  $^{12}\text{C}$  to  $^{208}\text{Pb}$ . The differential decay width shapes predicted for the two models are substantially different. Shell model distributions present discrete contributions and in the continuum appear sharp scattering resonances. Despite the fact that those

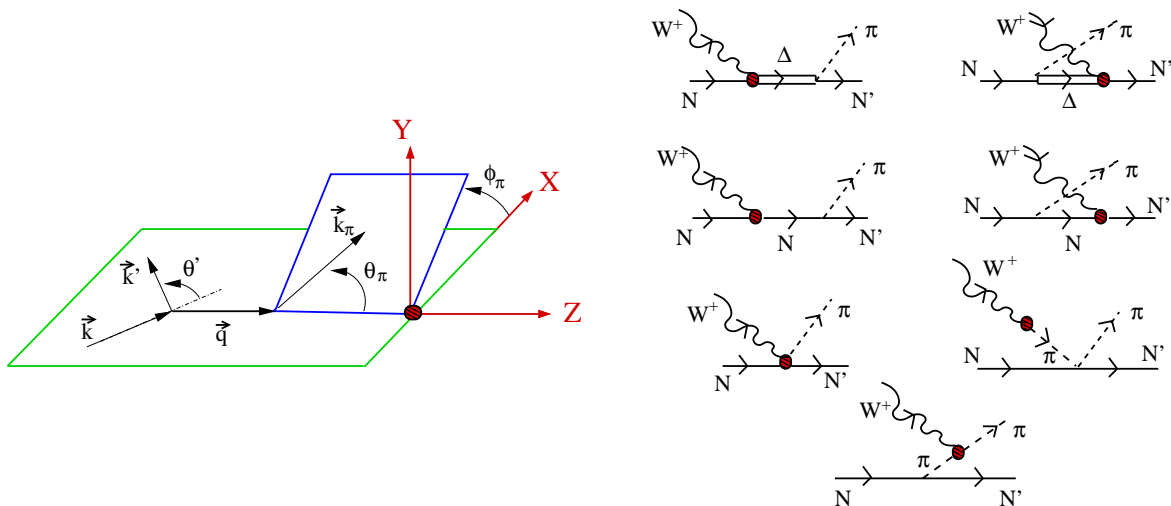


FIG. 2: Left: Definition of the kinematical variables used in this work. Right: Model for the  $W^+N \rightarrow N'\pi$  reaction. It consists of seven diagrams: Direct and crossed  $\Delta(1232)$ - (first row) and nucleon (second row) pole terms, contact and pion pole contribution (third row) and finally the pion-in-flight term. Throughout this work, we will label these contributions by:  $\Delta P$ ,  $C\Delta P$ ,  $NP$ ,  $CNP$ ,  $CT$ ,  $PP$  and  $PF$ , respectively. The circle in the diagrams stands for the weak transition vertex.

the final nucleus is left in a determined nuclear level. On the other hand, the LFG description of the nucleus allows for an accurate treatment of the dynamics of the elementary processes (interaction of gauge bosons with nucleons, nucleon resonances, and mesons, interaction between nucleons or between mesons and nucleons, etc.) which occur inside the nuclear medium. Within a finite nuclei scenario, such a treatment becomes hard to implement, and often the dynamics is simplified in order to deal with more elaborated nuclear wave functions.

### C. The virtual $W$ -self-energy in pion production: $1p1h1\pi$ contribution

In this subsection, we calculate the contribution to the cross section from  $W^+$  gauge boson self-energy diagrams which contains pion production in the intermediate states. We will use the model for the CC neutrino-pion production reaction off the nucleon,

$$\nu_l(k) + N(p) \rightarrow l^-(k') + N(p') + \pi(k_\pi) \quad (10)$$

derived in Refs. [32, 35]. This process, at intermediate energies, is traditionally described in the literature by means of the weak excitation of the  $\Delta(1232)$  resonance and its subsequent decay into  $N\pi$ . In Ref. [32], some background terms required by the pattern of spontaneous chiral symmetry breaking of QCD are also included. Their contributions are sizable and lead to significant effects in total and partially integrated pion production cross sections even at the  $\Delta(1232)$ -resonance peak, and they are dominant near pion threshold. The model consists of seven diagrams (right panel of Fig. 2). The contributions of the different diagrams are calculated by using the effective Lagrangian of the SU(2) nonlinear  $\sigma$ -model, supplemented with some form-factors (see Ref. [32] for details). In this work, we will use the set IV of form factors compiled in Table I of Ref. [35]. The available data set on neutrino and antineutrino pion production on nucleons is described reasonably well. Nonetheless, we must mention, that the experimental data still have large uncertainties and there exist conflicting data for some channels.

The discussed model can be considered an extension of that developed in Ref. [1] for the  $eN \rightarrow e'N\pi$  reaction. For the latter case, the model, that contains a theoretically well founded description of the background amplitudes, provides the same level of accuracy [36] as the MAID model [46], which ensures its applicability to the leptoproduction processes at least up to  $W < 1.4$  GeV, being  $W$  the outgoing  $\pi N$  invariant mass.

---

distinctive features do not appear in the LFG differential decay widths, the totally integrated widths (inclusive observable) obtained from both descriptions of the process do not differ in more than 5 or 10%. The typical nuclear excitation energies in muon and radiative pion capture in nuclei are small, of the order of 20 MeV, and thus one expects that at higher excitation energies, where one should sum up over a larger number of nuclear final states, the LFG predictions for inclusive observables would become even more reliable.

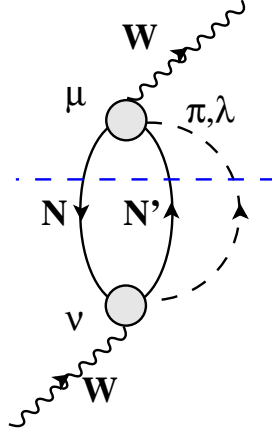


FIG. 3:  $W$ -self-energy obtained by folding the  $WN \rightarrow \pi N'$  amplitude ( $\lambda$  is the charge of the pion).

We move now to the computation of the  $W^+$  gauge boson self-energy diagrams which contain pion production in the intermediate states. This is readily accomplished by taking the  $W^+N \rightarrow \pi N'$  amplitude of Fig. 2 and folding it with itself. One gets then the diagram of Fig. 3 where the circle stands for any of the 7 terms of the elementary model for  $WN \rightarrow \pi N'$ . The solid lines going up and down in Fig. 3 follow the standard many body nomenclature and stand for particle and hole states respectively. The  $W$ -self-energy corresponding to this diagram (actually 49 diagrams) is readily evaluated and gives<sup>6</sup> (we will label it as 1p1h1 $\pi$ )

$$-i\Pi_{W;1\text{p}1\text{h}1\pi}^{\mu\nu}(q) = -i\left(\frac{g}{2\sqrt{2}}\right)^2 \sum_{N,N',\lambda} \int \frac{d^4k_\pi}{(2\pi)^4} \int \frac{d^4p}{(2\pi)^4} G(p; \rho_N) G(p'; \rho_{N'}) D_\pi(k_\pi) \times \text{Tr} \left( (\not{p} + M) \gamma^0 j_A^{\mu\dagger} \gamma^0 (\not{p}' + M) j_A^\nu \right) \quad (11)$$

$$= \left(\frac{g}{2\sqrt{2}}\right)^2 \sum_{N,N',\lambda} \int \frac{d^4k_\pi}{(2\pi)^4} \int \frac{d^3p}{(2\pi)^3} \frac{1}{2E(\vec{p})} \frac{1}{2E(\vec{p} + \vec{q} - \vec{k}_\pi)} \frac{n_N(\vec{p}) [1 - n_{N'}(\vec{p} + \vec{q} - \vec{k}_\pi)]}{q^0 - k_\pi^0 + E(\vec{p}) - E(\vec{p}') + i\epsilon} \times D_\pi(k_\pi) \text{Tr} \left( (\not{p} + M) \gamma^0 j_A^{\mu\dagger} \gamma^0 (\not{p}' + M) j_A^\nu \right) + [(q - k_\pi) \leftrightarrow -(q - k_\pi)] \quad (12)$$

where  $p' = p + q - k_\pi$ ,  $j_A^\mu$  is the amputated amplitude<sup>7</sup> for the  $W^+N \rightarrow N'\pi^\lambda$  process, which is obtained by summing up the contributions of all diagrams of the right panel of Fig. (2). The contribution to  $j_A^\mu$  of each diagram is given by their relation to the full amplitudes given in Eq. (51) of Ref. [32],

$$j_{cc+}^\mu \Big|_i = \bar{u}(\vec{p}') j_{A_i}^\mu(p, q, p' = p + q - k_\pi, k_\pi) u(\vec{p}), \quad i = \Delta P, C\Delta P, NP, CNP, CT, PP, PF. \quad (13)$$

The indices  $N, N'$  in Eq. (12) stand for the hole and particle nucleon states respectively and  $n_N(\vec{p}) = \Theta(k_F^N - |\vec{p}|)$  is the occupation number in the Fermi local sea, with  $k_F^N(r) = (3\pi^2 \rho_N(r))^{1/3}$  and  $\rho_N(r)$  the density of nucleons of a particular species  $N = n$  or  $p$  ( $\rho(r) = \rho_p(r) + \rho_n(r)$ ), normalized to the number of protons or neutrons. Besides,  $E(\vec{p})$  is the energy of the nucleon  $\sqrt{\vec{p}^2 + M^2} - k_F^2/2M$ , with  $M$  its mass and  $k_F(r) = (3\pi^2 \rho(r)/2)^{1/3}$ , and  $D_\pi$  is the pion propagator

$$D_\pi(k_\pi) = \frac{1}{k_\pi^2 - m_\pi^2 + i\epsilon} \quad (14)$$

with  $m_\pi$  the mass of the pion. Besides, the nucleon propagator in the medium reads,

$$S(p; \rho) = (\not{p} + M) G(p; \rho) \quad (15)$$

<sup>6</sup> In Eq. (11), it is necessary to subtract the free space contribution, i.e., the one that survives for vanishing nuclear densities. This contribution will renormalize free space couplings and masses. To obtain Eq. (12), we have neglected the contribution of the antiparticle pole ( $p^0 = -E(\vec{p}) - i\epsilon$ ) in the  $p^0$  integration, this also gets rid of the vacuum contribution that needed to be subtracted.

<sup>7</sup> The dependence of  $j_A^\mu$  on the  $N, N', \lambda$  channel is understood and it is not made explicit.

$$G(p; \rho) = \frac{1}{p^2 - M^2 + i\epsilon} + i \frac{\pi}{E(\vec{p})} n(\vec{p}) \delta(p^0 - E(\vec{p})) \quad (16)$$

$$= \frac{1}{p^0 + E(\vec{p}) + i\epsilon} \left( \frac{n(\vec{p})}{p^0 - E(\vec{p}) - i\epsilon} + \frac{1 - n(\vec{p})}{p^0 - E(\vec{p}) + i\epsilon} \right) \quad (17)$$

A further simplification can be done by evaluating the  $j_A^\mu$  amplitudes at an average momentum, which allows to take the spin trace in Eq. (12) out of the  $d^3\vec{p}$  integration. This latter integration can be now done, and it gives, up to some constants, the Lindhard function,  $\bar{U}_R(q - k_\pi, k_F^N, k_F^{N'})$  (see appendix B of Ref. [2]). We take  $\langle |\vec{p}| \rangle = \sqrt{\frac{3}{5}} k_F^N$  and a direction orthogonal to the plane defined by the pion and the virtual gauge boson. Within this approximation, we find

$$-i\Pi_{W;1\text{ph}1\pi}^{\mu\nu}(q) = \left( \frac{g}{2\sqrt{2}} \right)^2 \frac{1}{4M^2} \sum_{N,N',\lambda} \int \frac{d^4k_\pi}{(2\pi)^4} D_\pi(k_\pi) \bar{U}_R(q - k_\pi, k_F^N, k_F^{N'}) A^{\mu\nu}[\langle p \rangle, q, p' = \langle p \rangle + q - k_\pi, k_\pi] \quad (18)$$

$$A^{\mu\nu} = \frac{1}{2} \text{Tr} \left( (\langle \not{p} \rangle + M) \gamma^0 \langle j_A^{\mu\dagger} \rangle \gamma^0 (\langle \not{p} \rangle + \not{q} - \not{k}_\pi + M) \langle j_A^\nu \rangle \right) \quad (19)$$

where  $\langle j_A^\nu \rangle$  stands for  $j_A^\nu$  calculated with the average hole momentum  $\langle \vec{p} \rangle$ . To find the contribution to the hadron tensor  $W^{\mu\sigma}$  of the many body diagrams depicted in Fig. 3, we remind that by construction

$$A^{\mu\nu} = A_s^{\mu\nu} + iA_a^{\mu\nu} \quad (20)$$

with  $A_s^{\mu\sigma}$  ( $A_a^{\mu\sigma}$ ) real symmetric (antisymmetric) tensors, and thus

$$\text{Im} \left[ \Pi_{W;1\text{ph}1\pi}^{\mu\nu} + \Pi_{W;1\text{ph}1\pi}^{\nu\mu} \right] = 2\text{Im} \Pi_{W;1\text{ph}1\pi}^{\mu\nu} \Big|_s, \quad \text{Re} \left[ \Pi_{W;1\text{ph}1\pi}^{\mu\nu} - \Pi_{W;1\text{ph}1\pi}^{\nu\mu} \right] = -2\text{Im} \Pi_{W;1\text{ph}1\pi}^{\mu\nu} \Big|_a \quad (21)$$

where  $\Pi_{W;1\text{ph}1\pi}^{\mu\nu} \Big|_{s(a)}$  is defined as in Eq.(19), but replacing the full tensor  $A^{\mu\nu}$  by its symmetric (antisymmetric)  $A_s^{\mu\nu}$  ( $A_a^{\mu\nu}$ ) parts. The imaginary part of  $\Pi_{W;1\text{ph}1\pi}^{\mu\nu} \Big|_{s(a)}$  can be obtained by following the prescription of the Cutkosky's rules. In this case we cut with a straight horizontal line the intermediate particle and hole states and the pion. Those states are then placed on shell by taking the imaginary part of the propagator. Technically the rules to obtain  $\text{Im} \Pi_{W;1\text{ph}1\pi}^{\mu\nu} \Big|_{s(a)}$  reduce to making the substitutions:

$$\Pi_W^{\mu\nu}(q) \rightarrow 2i\text{Im} \Pi_W^{\mu\nu}(q) \Theta(q^0) \quad (22)$$

$$D_\pi(k_\pi) \rightarrow 2i\text{Im} D_\pi(k_\pi) \Theta(k_\pi^0) = -2\pi i \delta(k_\pi^2 - m_\pi^2) \Theta(k_\pi^0) \quad (23)$$

$$\bar{U}_R(q - k_\pi, k_F^N, k_F^{N'}) \rightarrow 2i\text{Im} \bar{U}_R(q - k_\pi, k_F^N, k_F^{N'}) \Theta(q^0 - k_\pi^0) \quad (24)$$

Thus, we readily obtain

$$W_{1\text{ph}1\pi}^{\mu\nu}(q) = -\Theta(q^0) \frac{1}{2M^2} \int \frac{d^3r}{2\pi} \sum_{N,N',\lambda} \frac{d^3k_\pi}{(2\pi)^3} \frac{\Theta(q^0 - k_\pi^0)}{2\omega(k_\pi)} \text{Im} \bar{U}_R(q - k_\pi, k_F^N, k_F^{N'}) A^{\nu\mu} \quad (25)$$

with  $\omega(k_\pi^0)$  the pion on-shell energy. The approximation done saves a considerable amount of computational time since there are analytical expressions for  $\text{Im} \bar{U}_R(q - k_\pi, k_F^N, k_F^{N'})$  [2]<sup>8</sup>.

---

<sup>8</sup> In the small density limit  $\text{Im} \bar{U}_R(q, k_F^N, k_F^{N'}) \simeq -\pi \rho_N M \delta(q^0 + M - \sqrt{M^2 + \vec{q}^2}) / \sqrt{M^2 + \vec{q}^2}$ . Substituting this into Eq. (25) one obtains

$$\lim_{\rho \rightarrow 0} W_{1\text{ph}1\pi}^{\mu\nu} \sim Z W_{W^+p \rightarrow p\pi^+}^{\mu\nu} + N \left( W_{W^+n \rightarrow p\pi^0}^{\mu\nu} + W_{W^+n \rightarrow n\pi^+}^{\mu\nu} \right) \quad (26)$$

being  $Z$  and  $N$  the number of protons and neutrons of the nucleus, and  $W_{W^+N \rightarrow N'\pi\lambda}^{\mu\nu}$  the hadronic tensor for CC pion production off the nucleon (see Eq. (4) of Ref. [32]). In this way, the strict impulse approximation is recovered. By performing the integral in Eq. (25), one accounts for Pauli blocking and for Fermi motion.

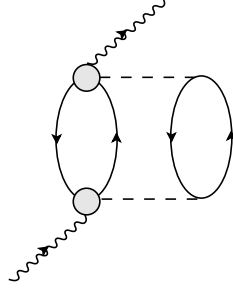


FIG. 4:  $W$ -self-energy obtained from the one in Fig. 3 when the pion line is allowed to excite a particle-hole.

#### D. The dip region: 2p2h absorption

In the two previous subsections we have discussed the dominant contributions to the inclusive  $\nu, \bar{\nu}$  nucleus CC cross section at low energies, namely QE scattering and pion production. In this subsection, we present a model for 2p2h mechanisms, which could be very relevant in the description of the region of transferred energies above the quasielastic and below the  $\Delta$ -resonance peaks (the dip region).

##### 1. 2p2h mechanisms driven by the longitudinal part of the effective spin-isospin $ph$ - $ph$ interaction

Let us consider again to the generic diagram of weak pion production of Fig. 3 and allow the pion to excite a particle-hole. This leads us to the diagram of Fig. 4. This is still a generic diagram which actually contains 49 diagrams when in the shaded circle we put each one of the terms of the  $WN \rightarrow \pi N$  amplitude of Fig. 2. The diagrams in Fig. 4 contribute to  $\text{Im}\Pi_W^{\mu\nu}$  according to Cutkosky rules when they are cut by a horizontal line, and the 2p2h are placed on shell. The contribution of the diagram of Fig. 4 can be obtained from that of Fig. 3, given in Eq. (12), by replacing ( $\Lambda_\pi = 1.2$  GeV,  $f_{\pi NN}^2/4\pi = 0.08$ )

$$D_\pi(k_\pi) \rightarrow D_\pi^2(k_\pi) F_\pi^4(k_\pi) \frac{f_{\pi NN}^2}{m_\pi^2} \vec{k}_\pi^2 U_\lambda(k_\pi), \quad F_\pi(k) = \frac{\Lambda_\pi^2 - m_\pi^2}{\Lambda_\pi^2 - k_\pi^2}, \quad (27)$$

where  $U_\lambda$  is the Lindhard function for a particle-hole excitation by an object of charge  $\lambda$ : this is, twice  $\bar{U}_R^{p,n}$  or  $\bar{U}_R^{n,p}$  for the excitation by a charged pion or  $\bar{U}_R^{p,p} + \bar{U}_R^{n,n}$  for the excitation by a neutral pion. The pion form factor  $F_\pi^4(k_\pi)$  appears because now the pions are off shell.

We can again simplify the expression by taking an average nucleon momentum of the Fermi sea to evaluate the amputated amplitudes for the  $W^+N \rightarrow N'\pi^+$  process. This allows us to factorize the Lindhard function and following the prescription of the Cutkosky's rules we get,

$$W_{2p2h}^{\mu\nu}(q) = \Theta(q^0) \frac{1}{M^2} \int \frac{d^3r}{2\pi} \sum_{N, N', \lambda} \int \frac{d^4k_\pi}{(2\pi)^4} \Theta(q^0 - k_\pi^0) F_\pi^2(k_\pi) \text{Im}\bar{U}_R(q - k_\pi, k_F^N, k_F^{N'}) A^{\nu\mu} \times \\ \times D_\pi^2(k_\pi) F_\pi^2(k_\pi) \frac{f_{\pi NN}^2}{m_\pi^2} \vec{k}_\pi^2 \Theta(k_\pi^0) \text{Im}U_\lambda(k_\pi) \quad (28)$$

Next, we have implemented several improvements that account for well established many body corrections:

1. In the above expression of Eq. (28), we have replaced

$$D_\pi^2(k_\pi) F_\pi^2(k_\pi) \frac{f_{\pi NN}^2}{m_\pi^2} \vec{k}_\pi^2 \text{Im}U_\lambda(k_\pi) \rightarrow \text{Im} \left( \frac{1}{k_\pi^2 - m_\pi^2 - \Pi(k_\pi)} \right) = \frac{\text{Im}\Pi}{|k_\pi^2 - m_\pi^2 - \Pi(k_\pi)|^2} \quad (29)$$

where for the selfenergy of a pion of charge  $\lambda$ , we have taken [41]

$$\Pi(k_\pi) = F_\pi^2(k_\pi) \frac{f_{\pi NN}^2}{m_\pi^2} \vec{k}_\pi^2 \frac{U(k_\pi)}{1 - \frac{f_{\pi NN}^2}{m_\pi^2} g' U(k_\pi)} \quad (30)$$



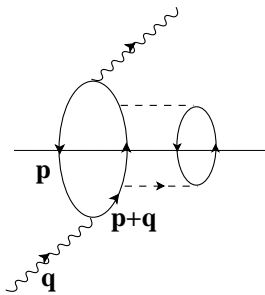


FIG. 5:  $W$ -selfenergy diagram obtained from the QE 1p1h excitation term (first of the diagrams depicted in Fig. 1) by dressing up the nucleon propagator of the particle state in the ph excitation.

where

$$U(k_\pi) = U_N(k_\pi) + U_\Delta(k_\pi) \quad (31)$$

is the non-relativistic Lindhard function for ph +  $\Delta$ h excitations<sup>9</sup> including direct and crossed bubbles [47, 48], in contrast to  $\bar{U}_R$  which only contains the direct bubble of a particle-hole excitation (the only one which contributes to  $\text{Im}U_N$  for  $q^0 > 0$ ). When evaluating  $\text{Im}\Pi(k_\pi)$  in the numerator of Eq. (29) we have not considered the part that arises from putting the  $\Delta$ h excitation on-shell that would correspond to a 2p2h+1 $\pi$  mechanism. We expect this latter contribution to be small at the considered energies. Note also, that by using  $U$  to compute the pion selfenergy, we have neglected small relativistic and  $\rho_p \neq \rho_n$  corrections. By means of Eq. (29), we have implemented the Dyson re-summation of the pion selfenergy, and have improved on this latter one by incorporating the Lorentz-Lorenz effect, driven by the short range Landau Migdal parameter  $g'$  [40], going in this way beyond 1p1h excitation<sup>10</sup> in the evaluation of  $\Pi(k_\pi)$ . We have used  $g' = 0.63$ , as in previous works [1, 2, 40, 41].

2. Let us now pay attention to the diagram of Fig. 5, which is already implicit in the generic diagram of Fig. 4 when the  $NP$  amputated amplitude is considered in both weak vertices. This  $W$ -selfenergy contribution can be obtained from the QE 1p1h excitation term (first of the diagrams depicted in Fig. 1) by dressing up the nucleon propagator of the particle state in the ph excitation. Indeed, this, among other contributions, was already taken into account in the QE study carried out in our previous work of Ref. [2], since there dressed nucleon propagators deduced from a realistic nucleon selfenergy [49] were used. To avoid double counting, we subtract the contribution of the  $NP$ - $NP$  diagram of Fig. 5 from Eq. (28).
3. When in one of the weak vertices of Fig. 4, the  $NP$  term is considered, the prescription of taking an average nucleon momentum of the Fermi sea used to obtain Eq. (28) turns out to be not appropriated. The reason is that when placing the 2p2h excitation on shell, through Cutkosky rules, we still have the nucleon propagator with momentum  $p + q$  (this is part of the amputated amplitude  $j_A^\mu|_{NP}$ ). This propagator can be still placed on shell for a virtual  $W$  and thus, there exists a single pole in the  $d^3p$  integration<sup>11</sup>. In this situation, one can not take an average for  $\vec{p}$ , as we have implicitly assumed in Eq. (28), and we have improved such prescription as follows. In this latter equation, it appeared the tensor  $A^{\nu\mu}$ , which in turn is defined in Eq. (19) by using an average for the hole three momentum  $\vec{p}$  to calculate both, the amputated  $WN \rightarrow N\pi$  amplitudes  $j_A^\mu$  and  $\not{p}$ , that also appears in the trace that defines  $A^{\nu\mu}$ . Instead of this, we have computed an average of the whole trace. To this end, we have numerically performed the integral over the angle formed by  $\vec{p}$  and  $\vec{q}$ , using still an average for the modulus of  $\vec{p}$  and taking this momentum in the XZ plane (recall that  $\vec{q}$  defines the Z-axis). All pathologies

<sup>9</sup> The functions  $U_N$  and  $U_\Delta$  are defined, e.g., in Eqs. (2.9) and (3.4) of Ref. [47].  $U_N$  incorporates a factor two of isospin with respect to  $\bar{U}_R$ , such that  $\text{Im}U_N = 2\text{Im}\bar{U}_R$  for symmetric nuclear matter, up to relativistic corrections.

<sup>10</sup> It corresponds to replace the ph excitation of the right-hand in Fig. 4 by a series of RPA excitations through ph and  $\Delta$ h excitations, driven by the longitudinal part of the effective spin-isospin interaction. In Subsect. IID2, we do something similar for the case of 2p2h mechanisms driven by  $\rho$ -meson exchange, and there we show graphically in Fig. 10 the RPA series, in that case induced by the transverse part of the effective spin-isospin interaction.

<sup>11</sup> This cut will also contribute to the nuclear response to the weak probe. But, while it will affect to the QE region, it is expected to be small and considerably difficult to calculate from the computational point of view (see Eq. (80) of Ref. [1]). Thus, for the sake of simplicity we have not considered such contribution.

arise from the  $p + q$  nucleon propagator hidden in the amputated amplitudes, which can be put on the mass shell, and thus the contribution of these diagrams depends critically on the angle formed by  $\vec{p}$  and  $\vec{q}$ , while it shows a very smooth dependence on the rest of kinematical variables of the hole momentum  $\vec{p}$ . Thanks to the approximations of using an average for the modulus of  $\vec{p}$  and fixing the  $(\vec{p}, \vec{q})$ -plane, we avoid to perform two nested integrals, with the obvious benefit in computation time. We have checked that the results are accurate at the level of 5–10%. To be more specific, in Eq. (28), we have replaced  $A^{\nu\mu}$  by

$$A^{\nu\mu} \Rightarrow \frac{1}{2} \int_{-1}^{+1} d\mu \frac{1}{2} \text{Tr} \left( (\not{p} + M) \gamma^0 j_A^{\nu\dagger} \gamma^0 (\not{p} + \not{q} - \not{k}_\pi + M) j_A^\mu \right) \quad (32)$$

with  $\mu = \vec{q} \cdot \vec{p} / |\vec{q}| |\vec{p}|$ . To speed up the numerical integration, we have also given a small width ( $\sim 10$  MeV) to the  $p + q$  nucleon. Results do not depend significantly on this choice.

For consistency, we have also performed this angular average for all contributions implicit in Fig. 4, though the prescription of using an average for  $\vec{p}$  leads to accurate results in all cases except those involving the  $NP$  amputated amplitude discussed above.

4. In the terms involving the  $NP$ , amputated amplitude (interferences with the rest of amplitudes of Fig. 1), there always appears a pion emitted after the  $WN$  vertex that couples to the second ph excitation (see for instance the line labeled as  $\pi$  in Fig. 6). There, one is assuming a pion exchange interaction among the two ph excitations. We have improved on that, and have replaced it by an effective longitudinal interaction,  $V_l$ ,

$$V_l(k) = \frac{f_{\pi NN}^2}{m_\pi^2} \left\{ F_\pi^2(k) \frac{\vec{k}^2}{k^2 - m_\pi^2} + g_l'(k) \right\}, \quad (33)$$

which besides pion exchange includes SRC driven by the Landau Migdal parameter  $g_l'(k)$  (see Refs. [40, 41, 48]). To achieve this, we have multiplied the amputated amplitude  $j_{ANP}^\mu$  by a suitable factor,

$$j_{ANP}^\mu \Rightarrow j_{ANP}^\mu \times \left( 1 + \frac{g_l'}{F_\pi^2 D_\pi \vec{k}_\pi^2} \right) \quad (34)$$

We have taken the same prescription also for those terms that include the  $CNP$ ,  $\Delta P$  and  $C\Delta P$  amputated amplitudes.

We have also considered the transverse channel interaction,  $V_t$ ,

$$V_t(k) = \frac{f_{\pi NN}^2}{m_\pi^2} \left\{ C_\rho F_\rho^2(k) \frac{\vec{k}^2}{k^2 - m_\rho^2} + g_t'(k) \right\}, \quad C_\rho = 2, \quad F_\rho(k) = \frac{\Lambda_\rho^2 - m_\rho^2}{\Lambda_\rho^2 - k^2}, \quad \Lambda_\rho = 2.5 \text{ GeV} \quad (35)$$

of the effective spin-isospin interaction among the two ph excitations. Here,  $m_\rho = 0.77$  GeV. The SRC functions  $g_l'$  and  $g_t'$  have a smooth  $k$ -dependence [38, 48], which we will not consider here<sup>12</sup>, and thus we will take  $g_l'(k) = g_t'(k) = g' = 0.63$ , as it was done in the study of inclusive nuclear electron scattering carried out in Ref. [1], and also in the previous work on the QE region of Ref. [2]. To account for such contribution to the 2p2h absorption cross section is slightly more complicated, because the tensor  $A^{\mu\nu}$  does not account for  $\rho$ -meson production in the primarily weak vertex. Details will be given in Subsect. IID 2.

The cut which places the two ph on shell in the diagrams of Fig. 4 is not the only possible one. In Fig. 7, we show a different cut (dotted line) which places one ph and the pion on shell. As done for real [37] and virtual [1] photons, we neglect this contribution in the non resonant terms, because at low energies where these pieces are important, the  $(W, \pi)$  channel is small and at high energies where the  $(W, \pi)$  contribution is important, this channel is dominated by the  $\Delta$  excitation and there this correction will be properly incorporated.

We have also considered two body diagrams, where each  $W$  boson couples to different bubbles (Fig. 8). Its contribution to the hadron tensor, taking average momenta for both hole nucleon momenta in first place, reads

<sup>12</sup> This is justified because taking into account the  $k$ -dependence leads to minor changes for low and intermediate energies and momenta, where this effective ph-ph interaction should be used.

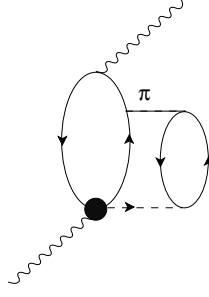


FIG. 6:  $W$ -selfenergy diagrams in which one of the vertices contains the  $NP$  term of the  $WN \rightarrow N\pi$  amplitude, while the other one (filled circle) contains all terms except that one.

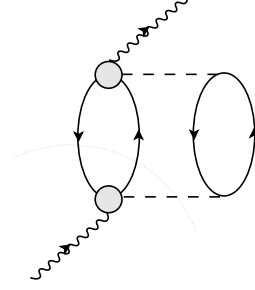


FIG. 7: Same as Fig. 4, showing the cut which places one particle-hole and the pion on shell.

$$W_{2p2h-2b}^{\mu\nu}(q) = -\Theta(q^0) \frac{1}{2\sqrt{2}M^4} \frac{f_{\pi NN}^2}{m_\pi^2} \int \frac{d^3r}{2\pi} \int \frac{d^4k_\pi}{(2\pi)^4} \Theta(k_\pi^0) \Theta(q^0 - k_\pi^0) F_\pi^4(k_\pi) \times \\ \times D_\pi(k_\pi) D_\pi(k_\pi - q) \text{Im} \bar{U}_R(k_\pi) \text{Im} \bar{U}_R(q - k_\pi) A_{2b}^{\nu\mu} \quad (36)$$

$$A_{2b}^{\mu\nu} = \frac{1}{2} \text{Tr} \left[ (\langle \not{p} \rangle + M) (\not{k}_\pi - \not{q}) \gamma_5 (\langle \not{p} \rangle + \not{q} - \not{k}_\pi + M) \underbrace{\langle j_A^\nu \rangle}_{W^+ p \rightarrow p\pi^+} \right] \times \\ \times \frac{1}{2} \text{Tr} \left[ (\langle \not{l} \rangle + M) \gamma^0 \underbrace{\langle j_A^{\mu\dagger} \rangle}_{W^+ n \rightarrow p\pi^0} \gamma^0 (\langle \not{l} \rangle + \not{k}_\pi + M) \not{k}_\pi \gamma_5 \right] + (W^+ n \rightarrow p\pi^0) (W^+ p \rightarrow p\pi^+) \\ - (W^+ n \rightarrow p\pi^0) (W^+ n \rightarrow n\pi^+) - (W^+ n \rightarrow n\pi^+) (W^+ n \rightarrow p\pi^0) \quad (37)$$

To compute this moderately small term, we have taken a proton-neutron symmetric Fermi sea, i.e.,  $k_F^p = k_F^n$ . We have labeled by  $p$  and  $l$ , the left and right bubble hole four momenta, and to compute  $\langle j_A^\nu \rangle$  and  $\langle j_A^{\mu\dagger} \rangle$ , the pion momenta are  $k_\pi$  and  $k_\pi - q$ , respectively. Besides, we write explicitly in Eq. (37) the sum over all charge combinations.

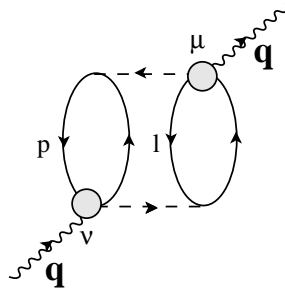


FIG. 8: Two particle-two hole  $W$ -selfenergy Feynman diagram where the outgoing gauge boson couples to the second nucleon.

Finally, we have improved on our evaluation of  $W_{2p2h-2b}^{\mu\nu}$  given in Eq. (37) by implementing also here the refinements 3 and 4, previously discussed, devoted to the improvements in the computation of  $W_{2p2h}$ . However, as in Ref. [1] for the inclusive electron-nucleus case, we have only considered the contributions stemming from the longitudinal part of the effective spin-isospin ph-ph interaction, driven by pion exchange (depicted in Fig. 8), and we have neglected those induced by the transverse one.

## 2. $2p2h$ mechanisms driven by the transverse part of the effective spin-isospin ph-ph interaction

In this subsection we evaluate the contribution to the weak nuclear response of the  $2p2h$  absorption terms driven by the transverse part of the effective spin-isospin ph-ph potential used in previous studies on electron [1], photon [37] and pion [38–42] interaction with nuclei. In the model of Ref. [38], this transverse interaction arises from  $\rho$ -exchange modulated by SRC. The major difficulty here, as compared with the previous works mentioned above, arises from the fact that we are using a relativistic description of the weak transition process. Thus, the first step is to model  $NN\rho$  and  $N\Delta\rho$  relativistic Lagrangians, which give rise, in the non-relativistic limit, to the transverse potential of Eq. (35). A convenient set of interaction Lagrangians is,

$$\begin{aligned}\mathcal{L}_{NN\rho} &= \frac{f_{\pi NN}}{m_\pi} \sqrt{C_\rho} \bar{\Psi} \sigma_{\mu\nu} \partial^\mu \bar{\rho}^\nu \cdot \vec{\tau} \Psi \\ \mathcal{L}_{N\Delta\rho} &= -i \frac{f_{\pi N\Delta}^*}{m_\pi} \sqrt{C_\rho} \bar{\Psi}_\nu \gamma_5 \gamma_\mu \vec{T}^\dagger \Psi (\partial^\mu \bar{\rho}^\nu - \partial^\nu \bar{\rho}^\mu) + \text{h.c.}\end{aligned}\quad (38)$$

where  $\Psi = \begin{pmatrix} p \\ n \end{pmatrix}$  is the nucleon field,  $\bar{\rho}^\nu$  is the  $\rho$ -meson Proca field<sup>13</sup>,  $\Psi_\nu$  is a Rarita Schwinger  $J^\pi = 3/2^+$  field,  $\vec{T}^\dagger$  is the isospin transition operator<sup>14</sup>,  $\vec{\tau}$  are the isospin Pauli matrices and  $f_{\pi N\Delta}^* = 2.14$ .

Next, we consider the  $W^+N \rightarrow N'\rho$  process and find the  $NP$ ,  $CNP$ ,  $\Delta P$  and  $C\Delta P$  amputated amplitudes obtained from the above Lagrangians. The Feynman diagrams for these four amplitudes are like those depicted in the right panel of Fig. 2 by replacing the outgoing pion by a  $\rho$ -meson. We will denote the amputated amplitudes by  $t_{A_i}^{\mu\alpha}$ . They are defined by

$$t_{cc+}^\mu \Big|_i = \bar{u}(\vec{p}') t_{A_i}^{\mu\alpha}(p, q, p' = p + q - k_\rho, k_\rho) u(\vec{p}) \epsilon_\alpha^*(k_\rho), \quad i = \Delta P, C\Delta P, NP, CNP \quad (39)$$

with  $\epsilon_\alpha^*$ , the  $\rho$ -meson polarization vector and  $t_{cc+}^\mu \Big|_i$  the full  $W^+N \rightarrow N'\rho$  amplitude for each mechanism. One readily finds that  $t_{cc+}^\mu \Big|_i$  can be obtained from the  $W^+N \rightarrow N'\pi$  amplitudes  $j_{cc+}^\mu \Big|_i$ , given in Eq. (51) of Ref. [32], with the following replacements deduced from the appropriate meson- $NN$  and meson- $N\Delta$  vertices,

$$\begin{aligned}NP \text{ and } CNP \text{ terms :} & \quad \not{k}_\pi \gamma_5 \Leftrightarrow \sqrt{C_\rho} k^\eta \sigma_{\eta\sigma} \epsilon^{*\sigma} \\ \Delta P \text{ term :} & \quad k_\pi^\alpha P_{\alpha\beta} \#^\beta \Leftrightarrow i \sqrt{C_\rho} \gamma_5 (\not{k} P_{\sigma\beta} - k^\alpha \gamma_\sigma P_{\alpha\beta}) \#^\beta \epsilon^{*\sigma} \\ C\Delta P \text{ term :} & \quad \#^\alpha k_\pi^\beta P_{\alpha\beta} \Leftrightarrow -i \sqrt{C_\rho} \#^\alpha (P_{\alpha\sigma} \gamma_5 \not{k} - P_{\alpha\eta} k^\eta \gamma_5 \gamma_\sigma) \epsilon^{*\sigma}\end{aligned}\quad (40)$$

where  $k$  is now the  $\rho$ -meson momentum ( $p + q = p' + k$ ). Now, we can compute the contribution of the 16 diagrams of Fig. 9 to the inclusive neutrino-nucleus cross section, when the two ph excitations are put on shell. The corresponding contribution to the hadron tensor reads, with the approximations discussed in the previous sections in order to factorize two Lindhard functions,

$$\begin{aligned}W_{2p2h-t}^{\mu\nu}(q) &= -\Theta(q^0) \frac{1}{M^2} \int \frac{d^3r}{2\pi} \sum_{N, N', \lambda} \int \frac{d^4k}{(2\pi)^4} \Theta(q^0 - k^0) F_\rho^2(k) \text{Im} \bar{U}_R(q - k, k_F^N, k_F^{N'}) B^{\nu\mu} \times \\ &\quad \times D_\rho^2(k) F_\rho^2(k) C_\rho^2 \frac{f_{\pi NN}^2}{m_\pi^2} \vec{k}_\pi^2 \Theta(k^0) \text{Im} U_\lambda(k)\end{aligned}\quad (41)$$

<sup>13</sup> Here  $\rho^\mu = (\rho_1^\mu - i\rho_2^\mu)/\sqrt{2}$  creates a  $\rho^-$  from the vacuum or annihilates a  $\rho^+$  and the  $\rho_3^\mu$  field creates or annihilates a  $\rho^0$ .

<sup>14</sup> It is a vector under isospin rotations and its Wigner-Eckart irreducible matrix element is taken to be one.

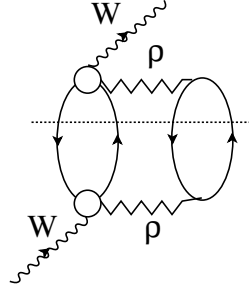


FIG. 9: Two particle–two hole  $W$ –selfenergy Feynman diagram driven by  $\rho$ –exchange. The cut (dotted line) that places the 2p2h on-shell is also displayed. The empty circle contains the direct and crossed nucleon and  $\Delta$ –pole terms of the  $WN \rightarrow N\rho$  amplitude.

with<sup>15</sup>  $D_\rho(k) = 1/(k^2 - m_\rho^2)$ . The form factor  $F_\rho^4(k)$ , Eq. (35), appears because the  $\rho$ 's are off shell. Also here, when placing the 2p2h excitations on shell, we have that the nucleon propagator with momentum  $p + q$  (this is part of the amputated amplitude  $t_A^{\mu\alpha}|_{NP}$ ) can be placed on shell for a virtual  $W$ . Thus, as discussed above in Eq. (32), we define the tensor  $B^{\nu\mu}$  as an angular average of the traces that appear in the evaluation of the diagram. Namely,

$$B^{\nu\mu} = \frac{1}{2} \int_{-1}^{+1} d\mu \frac{1}{2C_\rho} \text{Tr} \{ (\not{p} + M) \gamma^0 (t_A)_{\alpha}^{\nu\dagger} \gamma^0 (\not{p} + \not{q} - \not{k} + M) (t_A)^{\mu\alpha} \} \quad (42)$$

with  $\mu = \vec{q} \cdot \vec{p} / |\vec{q}| |\vec{p}|$ . To simplify the numerical integration, we have given a small width ( $\sim 10$  MeV) to the  $p + q$  nucleon and have used an average for the modulus of  $\vec{p}$  and fixed the  $(\vec{p}, \vec{q})$ –plane, avoiding thus to perform two nested integrals. The total  $W^+N \rightarrow N'\rho$  amputated  $t_A^{\mu\alpha}$  amplitude is obtained by summing those corresponding to the  $NP$ ,  $CNP$ ,  $\Delta P$  and  $C\Delta P$  mechanisms.

To deduce Eq. (41), we have approximated the ph  $\rho$ –selfenergy (right-hand part of the diagram depicted in Fig. 9) by

$$\Pi_{\alpha\beta} = (-g_{\alpha\beta} + k_\alpha k_\beta / k^2) \hat{\Pi}^\lambda, \quad \hat{\Pi}^\lambda(k) = F_\rho^2(k) C_\rho \frac{f_{\pi NN}^2}{m_\pi^2} \vec{k}^2 U_\lambda(k) \quad (43)$$

with  $\lambda$  the charge of the  $\rho$ –meson. Eq. (43) is obtained by neglecting higher order terms,  $\mathcal{O}(\vec{l}^2/M^2)$ , being  $\vec{l} = \vec{p}, \vec{q}$  or  $\vec{k}$ . This is consistent with the non-relativistic reduction that leads to the effective potentials in Eqs. (33) and (35).

As previously done, we also

- replace in Eq. (41),

$$\text{Im}U_\lambda(k) \Rightarrow \frac{\text{Im}U_\lambda(k)}{|1 - U(k)V_t|^2} \quad (44)$$

By including the non-relativistic Lindhard function for ph +  $\Delta$ h excitations in the denominator, we replace the ph excitation of the right-hand in Fig. 9 by a series of RPA excitations through ph and  $\Delta$ h excitations, driven by  $V_t$ , as depicted in Fig. 10 (some more details will be given below in the discussion of Eq. (57)).

- multiply  $t_A^{\mu\alpha}$  by a factor

$$t_A^{\mu\alpha} \Rightarrow t_A^{\mu\alpha} \times \left( 1 + \frac{g'_t}{F_\rho^2 D_\rho C_\rho \vec{k}^2} \right) \quad (45)$$

which allows us to replace the  $\rho$ –exchange interaction in Fig. 9 by the transverse part ( $V_t$ ) of the effective ph–ph potential.

Finally, and to avoid double counting we must subtract the  $NP$ – $NP$  contribution from Eq. (41), because this term was already taken into account in the evaluation of the QE contribution, through the inclusion of a realistic nucleon selfenergy, carried out in Ref [2].

<sup>15</sup> This is part of the  $\rho$ –meson propagator, that reads  $(-g^{\mu\nu} + k^\mu k^\nu / m_\rho^2) D_\rho$ . Actually, only the piece proportional to  $g^{\mu\nu}$  contributes since  $t_{A_i}^{\mu\alpha} k_\alpha = 0$ .

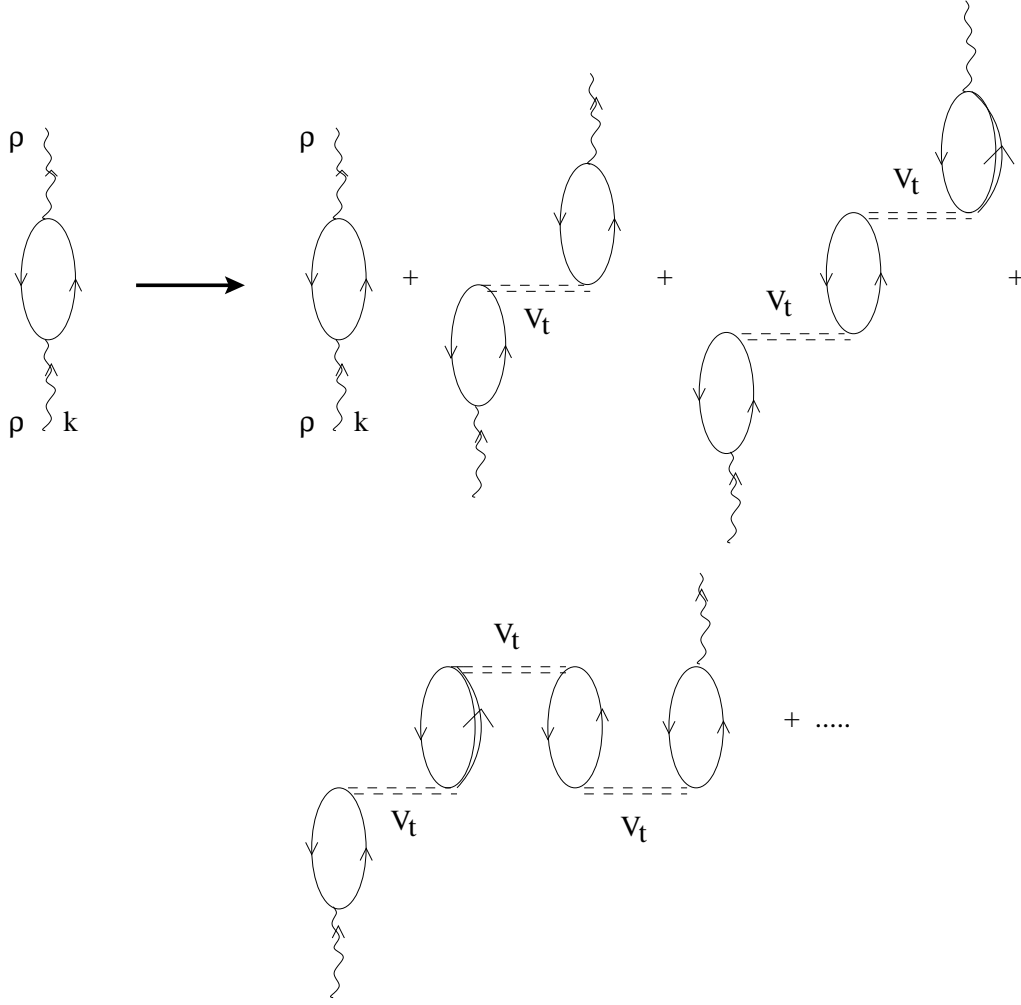


FIG. 10: Diagrammatic representation of a series of RPA excitations through ph and  $\Delta$ h excitations, driven by  $V_t$ .

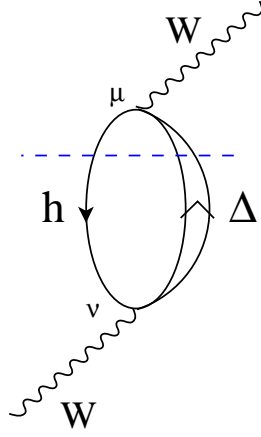
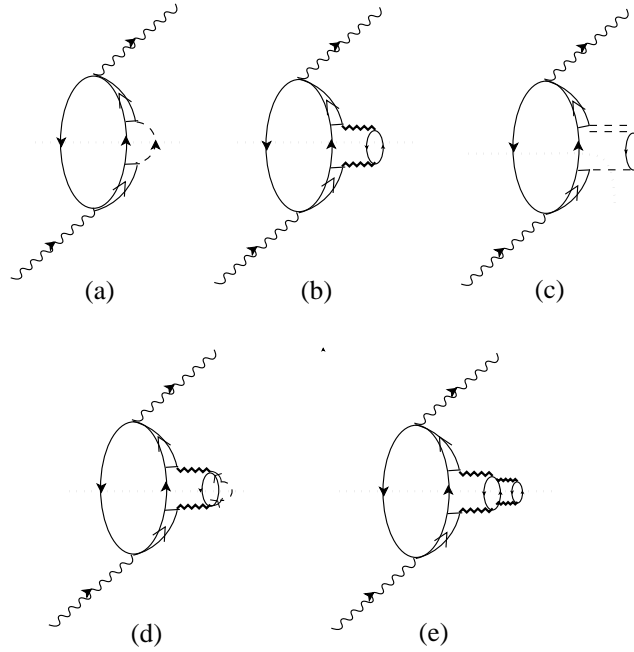
### E. The $\Delta$ excitation term

Like in pion-nuclear, photo-nuclear and electro-nuclear reactions at intermediate energies, the excitation of the  $\Delta(1232)$  resonance by the weak probe is expected to play a major role. This term is depicted in Fig. 11, and its contribution to the in medium  $W^+$ -selfenergy reads

$$\begin{aligned}
 -i\Pi_{W^+;\Delta h}^{\mu\nu}(q) &= -2\cos^2\theta_C \left(\frac{g}{2\sqrt{2}}\right)^2 \sum_N C_N^2 \int \frac{d^4p}{(2\pi)^4} \frac{1}{p_\Delta^2 - M_\Delta^2 + iM_\Delta\Gamma_\Delta} i\frac{\pi}{E(\vec{p})} n_N(\vec{p}) \delta(p^0 - E(\vec{p})) A_\Delta^{\mu\nu}(p, q), \\
 A_\Delta^{\mu\nu} &= \frac{1}{2} \text{Tr}((\not{p} + M)\gamma^0(\Gamma^{\alpha\mu})^\dagger\gamma^0 P_{\alpha\beta}\Gamma^{\beta\nu}),
 \end{aligned} \tag{46}$$

with  $p_\Delta = p + q$ ,  $M_\Delta$  the resonance mass and  $\Gamma_\Delta$  its width, which can be found, e.g., in Eq. (45) of Ref. [32]. The isospin factor  $C_N$  takes the values 1 and  $\sqrt{3}$  for neutron and proton hole contributions, respectively. Finally,  $P^{\mu\nu}(p_\Delta)$  is the spin 3/2 on-shell projection operator

$$P^{\mu\nu}(p_\Delta) = -(\not{p}_\Delta + M_\Delta) \left[ g^{\mu\nu} - \frac{1}{3}\gamma^\mu\gamma^\nu - \frac{2}{3}\frac{p_\Delta^\mu p_\Delta^\nu}{M_\Delta^2} + \frac{1}{3}\frac{p_\Delta^\mu\gamma^\nu - p_\Delta^\nu\gamma^\mu}{M_\Delta} \right] \tag{47}$$

FIG. 11: Diagrammatic representation of the  $\Delta h$  weak-nuclear excitation term.FIG. 12: Diagrammatic representation of the different contributions of the  $\Delta h$  weak-nuclear excitation term.

and  $\Gamma^{\alpha\nu}(p, q)$  is the weak  $N\Delta$  transition vertex, that can be found in Eq. (40) of Ref. [32]. The contribution to the hadron tensor from the selfenergy of Eq. (46) is<sup>16</sup>

$$W_{\Delta h}^{\mu\nu}(q) = -2 \cos^2 \theta_C \Theta(q^0) \sum_N C_N^2 \int \frac{d^3 r}{2\pi} \frac{d^3 p}{(2\pi)^3} \frac{n_N(\vec{p})}{E(\vec{p})} \text{Im} \left( \frac{1}{p_\Delta^2 - M_\Delta^2 + iM_\Delta \Gamma_\Delta} \right) A_\Delta^{\nu\mu} \Big|_{p^0=E(\vec{p})} \quad (48)$$

Some remarks are here in order. For instance, we must be careful to avoid double counting. Indeed, the contribution to the hadron tensor of the  $\Delta h$  excitation term arises from the imaginary part of the  $\Delta$  propagator, and in particular from the  $\Delta$ -width. One of the terms implicit in Eq. (12), the one where one picks up the  $\Delta$  excitation term both in  $j_A^\nu$  and in  $j_A^{\dagger\mu}$  (depicted diagrammatically in Fig. 12(a)), gives precisely the same contribution plus some medium corrections that take into account the Pauli blocking effects. Thus, if we would naively add it to the hadronic tensor, the contribution of Eq. (48) would be counted twice. Indeed, the term of Fig. 12(a) can be cast in the form of the

<sup>16</sup> Note that the tensor  $A_\Delta^{\mu\nu}$  can be split as in Eq. (20).

diagram of Fig. 11, but with a  $\Delta$ -selfenergy insertion constructed from a pion loop. When the pion is put on the mass shell to build the hadron tensor, we obtain the  $\Delta$ -width and thus qualitatively the equivalence is shown<sup>17</sup>. In a similar way, the diagram of Fig. 12(b) is one of the terms implicit in the diagram of Fig. 4 that produces a 2p2h excitation.

However, given the importance of the  $\Delta$ -pole contribution and since the  $\Delta$  properties are strongly modified inside the nuclear medium [1, 38, 40, 48, 51–53], a more careful treatment of the  $\Delta$  mechanisms is advisable. This implies some additional nuclear corrections to Eq. (48) to include the full effect of the self-energy of the  $\Delta$  in the medium  $\Sigma_\Delta(\rho(\vec{r}))$  in a systematic manner. In addition, these corrections provide genuinely new contributions to the hadronic tensor (e.g. 3p3h mechanisms). Here, we follow the same approach as in Ref. [1], which is based on Refs. [40, 41, 48]. In the nuclear medium the resonance self-energy is modified because of several effects such as Pauli blocking of the final nucleon and absorption processes:  $\Delta N \rightarrow NN$ ,  $\Delta N \rightarrow NN\pi$ , or  $\Delta NN \rightarrow NNN$ . This is done using a p-ph interaction that includes, besides pion exchange, SRC, a transverse channel driven by  $\rho$ -exchange (see Eq. (56)) and a RPA-re-summation.

Following this approach, in the  $\Delta$ -propagator, we approximate

$$\frac{1}{p_\Delta^2 - M_\Delta^2 + iM_\Delta\Gamma_\Delta} \sim \frac{1}{\sqrt{s} + M_\Delta} \frac{1}{\sqrt{s} - M_\Delta + i\Gamma_\Delta/2} \quad (55)$$

with  $s = p_\Delta^2$ . In the particle propagator of the right hand side of the above equation, we make the substitution:  $\Gamma_\Delta/2 \rightarrow \Gamma_\Delta^{\text{Pauli}}/2 - \text{Im}\Sigma_\Delta$  and take  $\text{Im}\Sigma_\Delta(\rho(\vec{r}))$  and  $\Gamma_\Delta^{\text{Pauli}}/2$  as follows. First, the Pauli blocking<sup>18</sup> of the  $\pi N$  decay reduces the  $\Gamma_\Delta$  free width to  $\Gamma_\Delta^{\text{Pauli}}$ , which can be found in Eq. (15) of Ref. [41]. Next, the imaginary part

<sup>17</sup> More quantitatively, to evaluate this term we can start from Eq. (11) and perform the  $d^4k_\pi$  integration in order to show explicitly the  $1\pi$   $\Delta$ -selfenergy  $\Sigma_\pi^{\alpha\beta}$ . We get

$$\begin{aligned} -i\Pi_{W;1\text{ph}1\pi}^{\mu\nu}\Big|_\Delta(q) &= -2i\cos^2\theta_C \left(\frac{g}{2\sqrt{2}}\right)^2 \sum_N C_N^2 \int \frac{d^4p}{(2\pi)^4} \frac{G(p;\rho_N)}{|(p+q)^2 - M_\Delta^2 + iM_\Delta\Gamma_\Delta|^2} \times \\ &\times \frac{1}{2} \text{Tr} \left( (\not{p} + M)\gamma^0(\Gamma^{\alpha\mu})^\dagger \gamma^0 P_{\alpha\beta}(-i\Sigma_{\Delta;\pi}^{\beta\delta}) P_{\delta\epsilon} \Gamma^{\epsilon\nu} \right) \end{aligned} \quad (49)$$

$$-i\Sigma_{\Delta;\pi}^{\beta\delta}(p_\Delta) = -\left(\frac{f_{\pi N\Delta}^*}{m_\pi}\right)^2 \int \frac{d^4k_\pi}{(2\pi)^4} D_\pi(k_\pi) k_\pi^\beta k_\pi^\delta G(p+q-k_\pi; \rho) (\not{p} + \not{q} - \not{k}_\pi + M) \quad (50)$$

where  $f_{\pi N\Delta}^* = 2.14$  is the  $\pi N\Delta$  coupling, and for simplicity we have evaluated the  $\Delta$ -selfenergy for a symmetric Fermi sea. In principle, the  $\Delta$ -selfenergy  $\Sigma_{\Delta;\pi}^{\beta\delta}$ , which is a matrix in the Dirac space and a Lorentz tensor can be expressed in terms of a linear combination of the five orthogonal spin projection operators introduced in Eq. (10) of Ref. [50]. The coefficients,  $A_i$  of such linear combination will be matrices in the Dirac space and Lorentz scalars. We will enormously simplify the discussion here neglecting  $\Delta$ -offshell effects. Within this approximation, the spin 3/2 projector of Ref. [50] reduces to that used here ( $-P^{\mu\nu}/2M_\Delta$ ) to construct the  $\Delta$ -propagator which satisfies  $P^{\mu\nu}P_{\nu\delta} = -2M_\Delta P_\delta^\mu$  and  $\not{p}P^{\mu\nu} = P^{\mu\nu}\not{p} = M_\Delta P^{\mu\nu}$ . Since in Eq. (49),  $\Sigma_{\Delta;\pi}^{\beta\delta}$  always appears contracted with two projector operators, one realizes that using the orthogonality properties, only the scalar quantity  $\Sigma_{\Delta;\pi}$ , defined as

$$\Sigma_{\Delta;\pi}^{\beta\delta} = -\Sigma_{\Delta;\pi} P^{\beta\delta} + \underbrace{\dots}_{\perp P^{\beta\delta}} \quad (51)$$

will contribute in Eq. (49), which now gets simplified to

$$-i\Pi_{W;1\text{ph}1\pi}^{\mu\nu}\Big|_\Delta(q) = 2\cos^2\theta_C \left(\frac{g}{2\sqrt{2}}\right)^2 \sum_N C_N^2 \int \frac{d^4p}{(2\pi)^4} G(p;\rho_N) \frac{4M_\Delta^2 \Sigma_{\Delta;\pi}}{|(p+q)^2 - M_\Delta^2 + iM_\Delta\Gamma_\Delta|^2} A_\Delta^{\mu\nu}(p, q) \quad (52)$$

Thus, we recover Eq. (48) from Eq. (52) when we replace  $G(p;\rho_N)$  by  $i\frac{\pi}{E(\vec{p})} n_N(\vec{p})\delta(p^0 - E(\vec{p}))$  to get rid of the vacuum contribution, and consider the imaginary part of the  $\Delta$ -selfenergy in Eq. (52). This is because to obtain the hadron tensor it appears always  $\text{Im}\Sigma_{\Delta;\pi}$ , thanks to the symmetry properties of the tensor  $A_\Delta^{\mu\nu}$ , and by noting that

$$\text{Im}\Sigma_{\Delta;\pi} = \frac{\Gamma_\Delta}{4M_\Delta}, \quad (53)$$

up to density corrections which will account for Pauli blocking. This latter relation follows from the Dyson equation for the  $\Delta$  propagator, within the on-shell approximation we are using,

$$\frac{iP^{\mu\nu}}{p_\Delta^2 - M_\Delta^2} + \frac{iP_{\mu\beta}}{p_\Delta^2 - M_\Delta^2} (-i\Sigma_{\Delta;\pi}^{\beta\delta}) \frac{iP_{\delta\nu}}{p_\Delta^2 - M_\Delta^2} + \dots = \frac{iP^{\mu\nu}}{p_\Delta^2 - M_\Delta^2 + 4M_\Delta^2 \Sigma_{\Delta;\pi}} \quad (54)$$

<sup>18</sup> In the diagram (a) of Fig. 12 appears the factor  $n_N(\vec{p})(1 - n_{N'}(\vec{p} + \vec{q} - \vec{k}_\pi))$ , see Eq. (12).



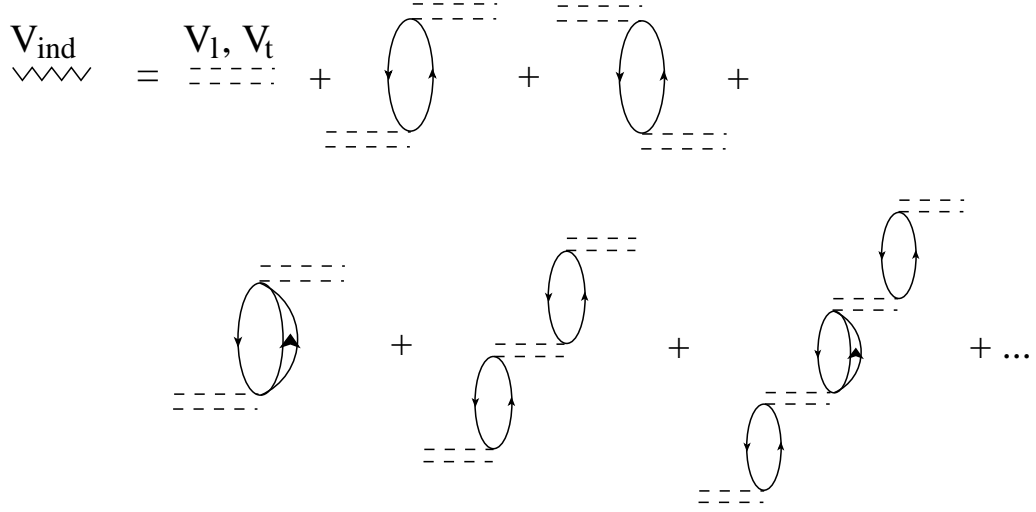


FIG. 13: Diagrammatic representation of the induced interaction.

of the selfenergy in Eq. (55) accounts for the diagrams depicted in Fig. 12, where the double dashed line stands for the effective spin–isospin interaction, while the wavy line accounts for the induced interaction. The effective spin–isospin interaction is originated by  $\pi$  and  $\rho$  exchange in the presence of short range correlations. It is obtained by substituting [40, 41, 48]

$$\left(\frac{f_{\pi NN}}{m_\pi}\right)^2 \hat{k}_i^\pi \hat{k}_j^\pi \vec{k}_\pi^2 D_\pi(k_\pi) \rightarrow \hat{k}_i^\pi \hat{k}_j^\pi V_l(k_\pi) + (\delta_{ij} - \hat{k}_i^\pi \hat{k}_j^\pi) V_t(k_\pi) \quad (56)$$

with  $\hat{k}_i^\pi = k_i^\pi / |\vec{k}_\pi|$ . The induced interaction accounts for the series of diagrams depicted in Fig. 13. There is an RPA sum through particle–hole and  $\Delta h$  excitations and it is readily obtained as

$$V_{\text{ind}} = \hat{k}_i^\pi \hat{k}_j^\pi \frac{V_l(k_\pi)}{1 - U(k_\pi)V_l(k_\pi)} + (\delta_{ij} - \hat{k}_i^\pi \hat{k}_j^\pi) \frac{V_t(k_\pi)}{1 - U(k_\pi)V_t(k_\pi)} \quad (57)$$

where  $U(k_\pi)$  is the non-relativistic Lindhard function for ph +  $\Delta h$  excitations<sup>19</sup> (see Eq. (31)). The evaluation of  $\Sigma_\Delta$  is done in Ref. [48]. The imaginary part of  $\Sigma_\Delta$  can be parametrized as

$$-\text{Im}\Sigma_\Delta(\rho(\vec{r})) = C_Q \left(\frac{\rho}{\rho_0}\right)^\alpha + C_{A_2} \left(\frac{\rho}{\rho_0}\right)^\beta + C_{A_3} \left(\frac{\rho}{\rho_0}\right)^\gamma \quad (58)$$

where the different coefficients are given<sup>20</sup> in Eq.(4.5) and Table 2 of Ref. [48]. The separation of terms in Eq. (58) is useful because the term  $C_Q$  comes from the  $\Delta N \rightarrow NN\pi$  process (diagrams (c) and (d) of Fig. 12 when the lines cut by the dotted line are placed on shell, and hence the term is related to the  $(W^*, \pi)$  channel), while  $C_{A_2}, C_{A_3}$  come from diagrams (b) and (e) and are related to two  $(W^*NN \rightarrow NN)$  and three  $(W^*NNN \rightarrow NNN)$  body absorption. Hence, the separation in this formula allows us to separate the final cross section into different channels.

To avoid double counting, we must subtract the contribution of the  $\Delta P$ – $\Delta P$  diagram of Fig. 12(a) from Eq. (19), already taken into account through the  $\Gamma_\Delta^{\text{Pauli}}$  piece of the  $\Delta$  selfenergy. We must also subtract the contribution of the  $\Delta P$ – $\Delta P$  diagram of Fig. 12(b) from Eqs. (28) and (41), because these terms were already taken into account in the evaluation of the  $C_{A_2}$  contribution to the  $\Delta$ –selfenergy [48].

<sup>19</sup> The different couplings for  $N$  and  $\Delta$  are incorporated in  $U_N$  and  $U_\Delta$  and then the same interaction strengths  $V_l$  and  $V_t$  are used for ph and  $\Delta h$  excitations [38].

<sup>20</sup> The parameterizations are given as a function of the kinetic energy in the laboratory system of a pion that would excite a  $\Delta$  with the corresponding invariant mass and are valid in the range  $85 \text{ MeV} < T_\pi < 315 \text{ MeV}$ . Below 85 MeV the contributions from  $C_Q$  and  $C_{A_3}$  are rather small and are taken from Ref. [41], where the model was extended to low energies. The term with  $C_{A_2}$  shows a very mild energy dependence and we still use the parametrization from Ref. [48] even at low energies. For  $T_\pi$  above 315 MeV we have kept these self-energy terms constant and equal to their values at the bound. The uncertainties in these pieces are not very relevant there because the  $\Delta \rightarrow N\pi$  decay becomes very large and absolutely dominant.

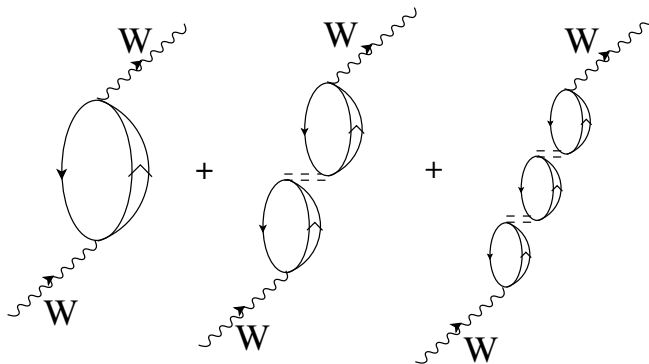


FIG. 14: Irreducible pieces in the  $\Delta h$  channel from the  $\Delta h$  interaction.

To end this subsection, we would like to devote a few words to the real part of the  $\Delta$ -selfenergy and the RPA sum of  $\Delta h$  excitations shown in Fig. 14. Both of them produce effects on the nuclear response to the weak probe that partially cancel out. In Ref. [48], the dispersive contributions to  $\text{Re}\Sigma_{\Delta}$  associated to the diagrams that gave rise to  $\text{Im}\Sigma_{\Delta}$  were also computed. There, it was found  $\text{Re}\Sigma_{\Delta}^{(0)} \sim -50\rho/\rho_0$  [MeV] at  $T_{\pi} = 50$  MeV and a smooth dependence on the pion energy. In principle,  $\text{Re}\Sigma_{\Delta}^{(0)}$  could be taken into account by substituting  $M_{\Delta} \rightarrow M_{\Delta} + \text{Re}\Sigma_{\Delta}^{(0)}$  in the particle propagator of the right hand side of Eq. (55). On the other hand, it is easy to realize that the RPA sum of  $\Delta h$  excitations, shown in Fig. 14 can be cast as a contribution to the real part of the  $\Delta$ -selfenergy [1]. Actually, the latter depends on the particular component of the hadron tensor  $W_{\Delta h}^{\mu\nu}$  which is being evaluated. Thus, for instance, the RPA series depicted in Fig. 14 can be taken into account, when computing  $W_{\Delta h}^{xx}$  or  $W_{\Delta h}^{yy}$  (transverse components to the direction of the  $W$ -boson) by replacing  $\text{Re}\Sigma_{\Delta}^{(0)}$  by  $\text{Re}\Sigma_{\Delta}^{(0)} + 4\rho V_t/9$ . This latter sum, in good approximation, is positive for the whole range of energies studied here. This was the situation for the inclusive  $(e, e')$  nuclear reaction studied in Ref. [1], since there, the excitation of the  $\Delta$  resonance by the virtual photon selected the transverse mode of the RPA series (see discussion of Eq. (44) in Ref. [1]). However, when the longitudinal component  $W_{\Delta h}^{zz}$  is evaluated, the longitudinal part,  $V_l$ , of the effective spin-isospin interaction is selected and now, this RPA sum is taken into account by substituting<sup>21</sup>  $\text{Re}\Sigma_{\Delta}^{(0)}$  by  $\text{Re}\Sigma_{\Delta}^{(0)} + 4\rho V_l/9$ , which shows a more pronounced  $q^2$  dependence than the combination that appeared in the RPA renormalization of transverse components of the hadronic tensor. Indeed, it turns out that the  $\text{Re}\Sigma_{\Delta}^{(0)} + 4\rho V_l/9$  combination does not have a well defined sign for the whole kinematical range of energies studied in this work. Setting to  $M_{\Delta}$  the position of the pole of the  $\Delta$  propagator, or changing it by adding or subtracting to  $M_{\Delta}$  about 30 MeV, as it could be inferred from the typical values that  $\text{Re}\Sigma_{\Delta}^{(0)} + 4\rho V_{l(t)}/9$  takes for the relevant kinematics to this work, leads to trivial shifts in the position of the  $\Delta$ -peak, moderately changes of the strength (around 20 %) at the maximum and very tiny changes of the  $q^0$ -differential shape. Of course, all these effects induced by the RPA-re-summation might be properly taken into account, as it was done for the case of the QE-region<sup>22</sup> in Ref. [2], but they, in conjunction with  $\text{Re}\Sigma_{\Delta}^{(0)}$ , would induce changes smaller than both, the precision in the current experimental determination of cross sections, and the uncertainties due to our lack of a precise knowledge of the axial nucleon-to- $\Delta$  transition form factor  $C_5^A$  [35]. For simplicity, in this work we will not renormalize the real part of the position of the  $\Delta$ -peak, which eventually could be studied in the future when more accurate measurements become available.

<sup>21</sup> Note that, in the studies of neutrino induced pion coherent production in nuclei carried out in Refs. [52, 53], the replacement  $\text{Re}\Sigma_{\Delta}^{(0)}$  by  $\text{Re}\Sigma_{\Delta}^{(0)} + 4\rho g'/9$  is employed to account for the corresponding RPA re-summations. The Landau Migdal parameter  $g'$  used there is part of  $V_l$ , which in addition also includes explicit pion-exchange (see Eq. (33)) [40, 41, 48]. This latter contribution was not considered in the works of Refs. [52–54], because there the distortion of the pion, by using an outgoing solution of the Klein-Gordon equation with the optical pion-nucleus potential derived in Ref. [41], was implemented, and it accounts for the RPA-renormalization induced by the  $\Delta h$ - $\Delta h$  pion-exchange interaction.

<sup>22</sup> For QE kinematics, taking into account properly the RPA effects is much more important [2] than in the  $\Delta$ -region, since the cancellation of their effects with the difference between particle and hole selfenergies is much less effective.

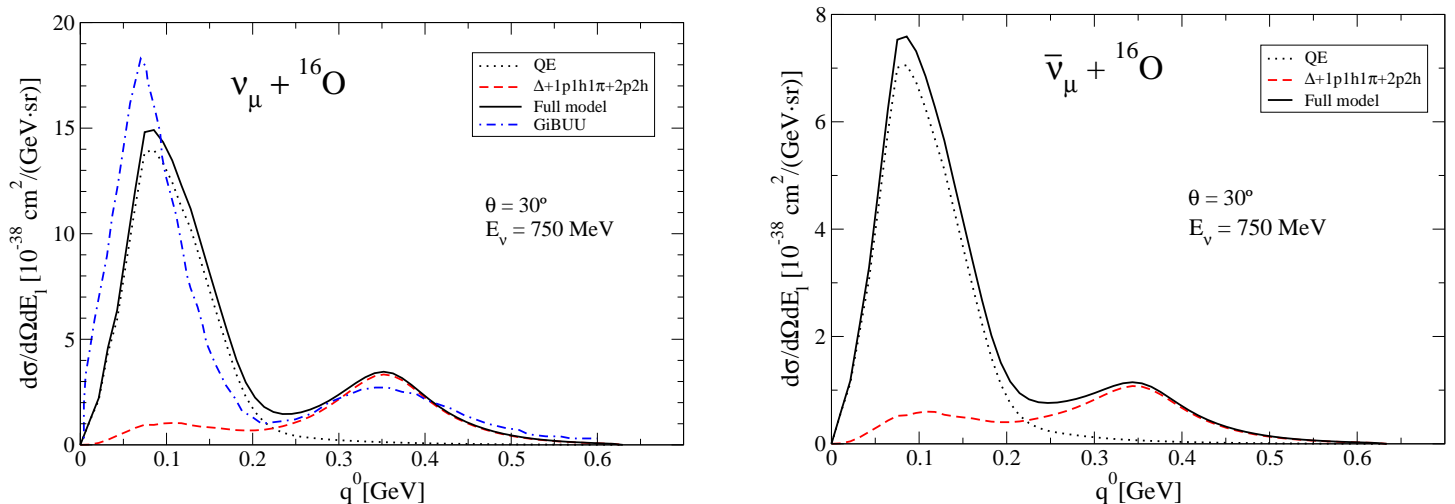


FIG. 15: Muon neutrino (left) and antineutrino (right) CC differential cross section  $\frac{d\sigma}{d\Omega dE_\mu}$  in oxygen, at 30 degrees of scattering angle and with an incident neutrino energy of 750 MeV, plotted against the transferred energy to the nucleus. Different contributions are displayed, standing the solid lines for our full model results. Besides in the left panel, we also show results (blue dash-dotted line) from Ref. [13] and obtained within the GiBUU framework.

### F. CC antineutrino induced reactions

The cross section for the antineutrino induced nuclear reaction

$$\bar{\nu}_l(k) + A_Z \rightarrow l^+(k') + X \quad (59)$$

is easily obtained from the expressions given in the previous subsections, by changing the sign of the antisymmetric part of the lepton tensor ( $L^a$ ) and using the  $W^-N \rightarrow N'\pi^\lambda$  amplitudes of Ref. [32], instead of those involving the  $W^+$  gauge boson. Note that the pion production off the nucleon amplitudes give rise, directly or indirectly, to all contributions considered here, except the QE ones. We take the  $\bar{\nu}$ -QE cross sections from Ref. [2].

## III. RESULTS

We will mainly focus here in the dip and  $\Delta$ -peak regions, since the QE contribution was discussed at length in Ref. [2]. In Fig. 15, we show results for both muon neutrino (left) and antineutrino (right) induced CC differential cross sections at 30 degrees as a function of the energy transferred to the nucleus ( $^{16}\text{O}$ ). The incoming neutrino (antineutrino) energy is 750 MeV. We clearly observe both the  $\Delta(1232)$  and the QE peaks; for this scattering angle, the QE contribution turns out to be significantly larger than that of the  $\Delta$  resonance. We split the full contribution into the QE and non QE ( $\Delta+1p1h1\pi+2p2h$ ) parts. General features are the same for both neutrino and antineutrino induced cross sections, and the main difference is an homogeneous reduction in the size of the differential cross section. For comparison, in the left panel (blue dashed-dotted line) we also display some results from Ref. [13], obtained within the Giessen Boltzmann-Uehling-Uhlenbeck (GiBUU) framework, which takes into account various nuclear effects: the local density approximation for the nuclear ground state, mean-field potentials, and in-medium spectral functions, but does not include those due to RPA correlations. We note first, some discrepancies between these results and ours in the QE region, which origin can be traced back to the implementation of RPA corrections in our scheme [2]. Indeed, the found differences (small shift in the position and reduction in size, about 25%, of the QE peak) are qualitatively identical to those existing between data and GiBUU predictions for the case of inclusive electron cross section for a similar kinematics (incident electron energy of 700 MeV and scattering angle of 32 degrees) showed in the upper panel of Fig. 9 of Ref. [13]. On the other hand, in this latter figure can be also appreciated the differences with the GiBUU model in the description of the dip region. Indeed, we see in Fig. 15 that in the dip region, our model predicts larger cross sections than those obtained within the GiBUU scheme. This is due to the 2p2h mechanisms of Figs. 4 and 9 included in our model. Actually, these contributions make also our cross section at the  $\Delta$ -peak larger than the one predicted in Ref. [13], even though we use a value of  $C_5^A(0)$  smaller than that used in Ref. [13] (1 vs 1.2). For larger scattering angles, the dip-region cross section becomes relatively much more important, and thus the

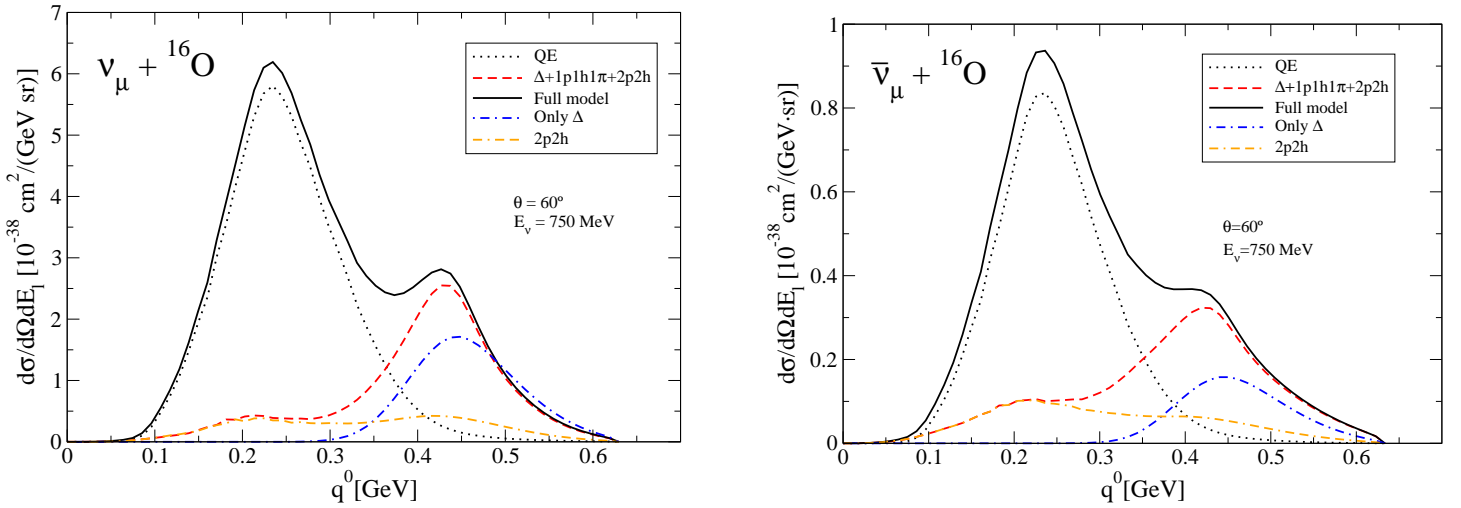


FIG. 16: Muon neutrino (left) and antineutrino (right) CC differential cross section  $\frac{d\sigma}{d\Omega dE_\mu}$  in oxygen, at 60 degrees of scattering angle and with an incident neutrino energy of 750 MeV, plotted against the transferred energy to the nucleus. The solid lines stand for our full model results.

inclusion of the 2p2h contributions turns out to be of larger relevance. This is clearly appreciated in Fig. 16, where we show results at 60 degrees. In this figure, besides the separation between QE and non QE contributions to the differential cross section, the 2p2h part<sup>23</sup> of this latter contribution is shown (orange double dash-dotted curves). The blue dash-dotted lines stand in this figure for the results obtained from only the  $\Delta$ h weak-nuclear excitation term of Fig. 12(a), neglecting Pauli blocking effects affecting the in medium resonance width. We see how the systematic many body  $W$ -absorption modes and the in medium effects considered here change drastically the nuclear response function in the  $\Delta$ -peak, as happened in the QE region as well [2].

The 2p2h cross section accounts for events where the gauge boson is absorbed by a pair of nucleons, in contrast to QE events for which it is absorbed by one nucleon, and furthermore no pions are being produced in this first step. Up to re-scattering processes which could eventually produce secondary pions, 2p2h events will give rise to only one muon to be detected. Thus, they could be experimentally misidentified as QE events. Yet, 1p1h1 $\pi$  events, in which the resulting pion from the  $W$  absorption is subsequently absorbed and does not come off the nucleus, could be also misinterpreted as QE events, if only leptons are being detected. A correct identification of CCQE events, which is the signal channel in oscillation experiments, is relevant for neutrino energy reconstruction and thus for the oscillation result. By looking at the 2p2h contribution in Fig. 16, we see that at least about 15% of the quasielastic cross section might be misidentified in present-day experiments and need to be corrected for by means of event generators. As mentioned above, 1p1h1 $\pi$  mechanisms followed by the absorption of the resulting pion, will even make worse the situation [55].

In Fig. 17, we show CC  $q^2$  differential cross sections in carbon for an incident energy of 1 GeV. We observe that the 2p2h contribution is sizeable for both, neutrino and antineutrino induced reactions, and that it shows a less pronounced  $q^2$  dependence than the QE or the  $\Delta + 1p1h1\pi$  components of the total result. On the other hand, the antineutrino distribution is much narrower than the neutrino one. Neglecting lepton mass effects, both distributions should be equal at  $q^2 = 0$ , and since the antineutrino cross sections are smaller than the neutrino ones, is reasonable to expect the  $\nu$  distributions to be wider than the  $\bar{\nu}$  ones.

The MiniBooNE collaboration has measured [3] the muon neutrino's CCQE cross section on  $^{12}\text{C}$ . The flux-unfolded results as a function of the neutrino energy are depicted in the left panel of Fig. 18, together with different predictions from the scheme presented here. The first observation is that our QE curve misses the data-points, being our predicted QE cross section significantly smaller than those reported by the MiniBooNE collaboration. Actually in [3], and to achieve a reasonable description of the data, an unexpectedly high effective axial mass  $M_A^{\text{eff}}$  (entering in the axial-vector  $WNN$  form-factor) of 1.35 GeV had to be used in the relativistic FG model implemented in the NUANCE event generator employed by the MiniBooNE collaboration. This value of  $M_A$  is significantly larger than the world average

<sup>23</sup> A small three body absorption (3p3h) contribution, induced by  $C_{A_3}$  in the  $\Delta$ -selfenergy of Eq. (58) is also included under the label 2p2h in Fig. 16, and in what follows.

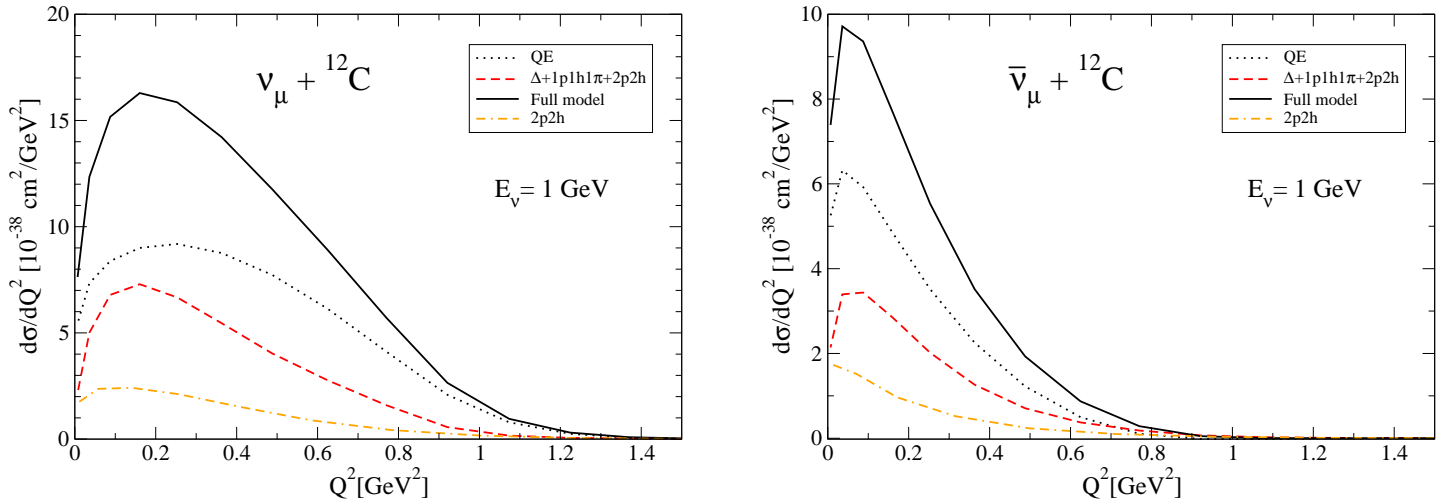


FIG. 17: Muon neutrino (left) and antineutrino (right) CC differential cross section  $\frac{d\sigma}{dQ^2}$  in carbon for an incident neutrino energy of 1 GeV ( $Q^2 = -q^2$ ). Different contributions are displayed, standing the solid lines for our full model results.

value  $M_A = 1.03$  GeV. It is interesting to note, however, that in Ref. [3] is also pointed out the NOMAD [24] and LSND [56] high energy ( $E_\nu > 4$  GeV) CCQE cross sections are better described with the world average value for  $M_A$ . The situation become even more worrying, after the work of Ref. [22]. That work finds that a theoretical approach based on the impulse approximation and realistic spectral functions, successfully applied to QE electron scattering, fails to reproduce the CCQE neutrino-nucleus cross section, unless the value of the nucleon axial mass resulting from deuteron measurements is significantly increased. In addition, they also rule out the possibility, advocated in Ref. [3], of interpreting the large  $M_A$  resulting from the MiniBooNE analysis as an effective axial mass, modified by nuclear effects beyond the FG model [57]. Actually, in [22], it is suggested that the many body techniques successfully applied in QE electron-nucleus scattering are not able to explain neutrino induced cross sections and it is argued that the development of a new *paradigm*, suitable for application to processes in which the lepton kinematics is not fully determined, will be required.

Our results do not support this last statement/interpretation, and we rather agree with the picture that emerges from the works of M. Martini et al. [27, 28]. These latter works, in our opinion, constituted a significant step forward to clarify the situation. As mentioned above, in the MiniBooNE analysis, ejected nucleons are not detected and the QE cross section is defined as the one for processes in which only a muon is detected in the final state. The MiniBooNE analysis of the data corrects (through a Monte Carlo estimate) for events, where in the neutrino interaction a pion is produced, but it escapes detection because it is reabsorbed in the nucleus, leading to multinucleon emission. However, in [27, 28] it is pointed out that 2p2h or 3p3h mechanisms are susceptible to produce an apparent increase in the “QE” cross section, since those events will give rise to only one muon to be detected, and the MiniBooNE analysis does not correct for them. Within the scheme followed in Ref. [22], the occurrence of 2p2h final states is described by the continuum part of the spectral function, arising from nucleon-nucleon correlations, and there, this contribution is found to be quite small (less than 10% of the integrated spectrum). This is not surprising, since our QE results (dashed line) in the left panel of Fig.18 contain also this contribution<sup>24</sup>, and as we mentioned, we underestimate the data. However, the 2p2h contribution considered in [22] is far from being complete<sup>25</sup> and it corresponds only to the many body diagram depicted in Fig. 5. Here, we compute all the contributions contained in the generic diagrams of Figs. 4, 8 and 9, as it was previously done in Ref. [1] for electron scattering, obtained from a realistic model for the weak pion production off the nucleon. When these latter contributions are added to the QE prediction of Ref. [2], we obtain the solid green line in the left plot of Fig.18 in a better agreement with the MiniBooNE data.

As commented before, these multinucleon knockout events are likely part of the CC“QE” cross section measured

<sup>24</sup> The CCQE cross sections calculated in Ref. [2], were obtained using both particle and hole dressed propagators, determined from a realistic in medium nucleon selfenergy [49], and thus account for the spectral function effects considered in [22].

<sup>25</sup> In fact, the spectral function model taken as a *paradigm* in the discussion of Ref. [22], though successful to account for the QE electron-nucleus scattering, at intermediate energies, badly fails to describe both the dip and the  $\Delta$ -regions, as can be appreciated for instance in Figs. 5-8 of Ref. [8] or in the Fig. 1 of Ref. [22]. This is because the lack of a proper model to account for the absorption of the virtual photon for two or three nucleons in that model.

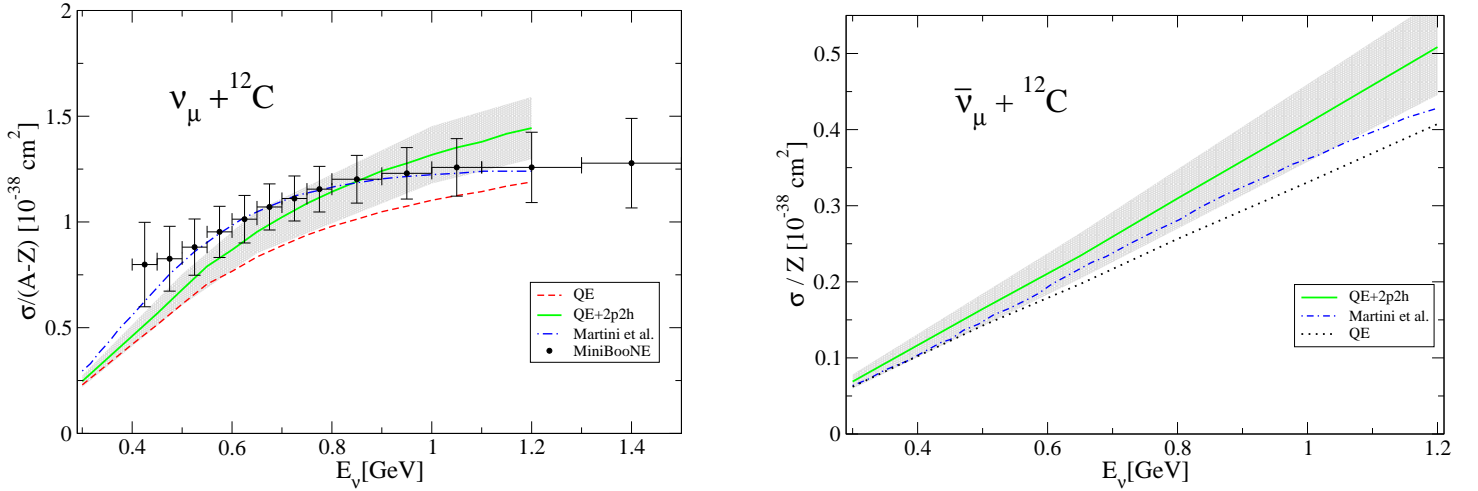


FIG. 18: Left: Flux-unfolded MiniBooNE  $\nu_\mu$  CCQE cross section per neutron as a function of neutrino energy (data-points) from Ref. [3], together with different theoretical predictions from this work. Right: Different theoretical calculations for antineutrino cross sections per proton off  ${}^{12}\text{C}$  as a function of the antineutrino energy. For comparison, in both plots, we also show the results (blue dash-dotted line) of Martini and collaborators taken from Ref. [28]. Bands accounting for the theoretical errors affecting our results are displayed in both panels.

by MiniBooNE, and that naturally explains the failure of the scheme of Refs. [8, 22].

Coming back to the left plot of Fig.18, there we also display the band of theoretical uncertainties affecting our results. To estimate this band, we have summed in quadratures a 15% relative error in our results with the error induced by the uncertainties on the parametrization of the  $C_5^A(q^2)$  form factor used here (set IV in Table I of Ref. [35]). As discussed in Ref. [43] for the CCQE case, 15% is a conservative ansatz to account for the errors, in total and differential inclusive cross sections, induced by the uncertainties affecting the nuclear corrections included in our model. Once, our theoretical uncertainties are taken into account, we find a reasonable agreement with the MiniBooNE data. We would like to stress that we have not fitted here any parameter, and that we have just extended our previous work on electron-scattering of Ref. [2] to the study of CCQE cross sections.

In Fig. 18, we also show the results of Martini and collaborators (blue dash-dotted line), taken from the  $QE+np-nh$  RPA curves of Fig. 5 of Ref. [28], which nicely fall within our band of theoretical predictions. Details of the model used by M. Martini and collaborators can be found in Ref. [27]. The evaluation of the nuclear response induced by these 2p2h mechanisms carried out in Ref. [27] is approximated, as explained there. The contributions in [27] that can be cast as a  $\Delta$ -selfenergy diagram should be quite similar to those obtained here in Subsect. II E, since in both cases the results of Ref. [48] for the  $\Delta$ -selfenergy are used. However, some other contributions included here are, either not considered or not properly taken into account in [27]. For example, we believe that none of diagrams of Fig. 8 or those in Fig. 4 involving the  $CT$ ,  $PP$  and  $PF$  vertices of Fig. 2 have been considered in the work of Martini and collaborators. Moreover, the  $NP-NP$ ,  $CNP-CNP$ ,  $NP-CNP$ ,  $NP-\Delta P$ ,  $NP-C\Delta P$ ,  $CNP-\Delta P$ ,  $CNP-C\Delta P$  and  $\Delta P-C\Delta P$  diagrams implicit in Fig. 4, are not directly evaluated in [27], but instead, an indirect estimate is given for them by relating their contribution to some absorptive part of the  $p$ -wave pion-nucleus optical potential. Given all this, we find remarkable the agreement exhibited in Fig. 18 between our results and those previously published in Refs. [27, 28].

On the other hand, we see that in our calculation the relative contribution of the 2p2h mechanisms with respect to the QE cross section, is quite similar for both neutrino and antineutrino induced processes. Thus, in what respect to this issue, our results do not support the claims of Ref. [28] on a minor role of the 2p2h mechanisms in the antineutrino mode.

We should mention that the MiniBooNE collaboration has also published the flux-integrated CC"QE" double differential cross section  $d^2\sigma/dE_\mu d\cos\theta_\mu$  in bins of muon energy  $E_\mu$  and cosine of the muon scattering angle with respect to the incoming neutrino direction. We must refrain to compare with these valuable data. The reason is that the MiniBooNE flux remains sizeable up to neutrino energies too high to make meaningful the predictions of the model presented here. Indeed, neutrino energies of 1 or 1.2 GeV at most, is the clear upper limit of validity of our predictions. The fraction of the MiniBooNE flux above 1.2 GeV is still larger than 17%, and this together with the fact that the cross sections grows with the energy has prevented us to do the comparison. We are working in extending our model to higher energies, but this is far from being a trivial task. New channels (2p2h1 $\pi$  or two pion production, ...) and higher resonances must be incorporated into the model, besides of smoothly getting rid of the

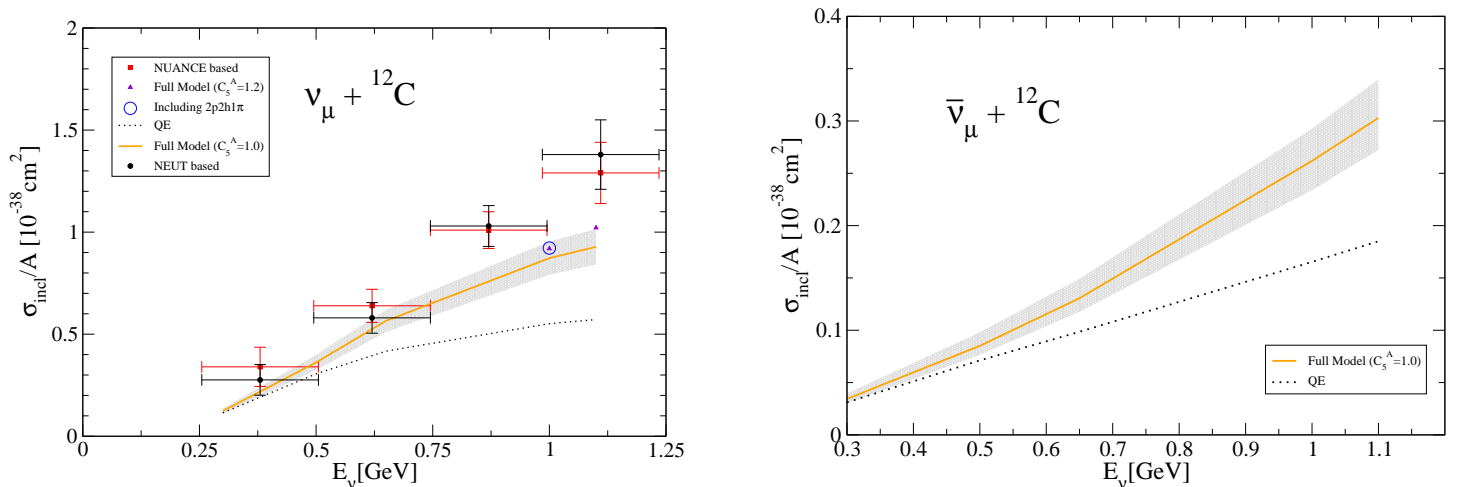


FIG. 19: Left: Data points stand for the SciBooNE neutrino CC inclusive interaction cross section per nucleon [6]. We also show our QE and full model results, and in this latter case the theoretical uncertainty band is also displayed. At 1 GeV, we depict the full model cross sections obtained when the GTR value of 1.2 for  $C_5^A(0)$  is used instead of 1 (violet triangle), and when some 2p2h1 $\pi$  contributions (blue empty circle), neglected in the present work, are taken into account (see text for some more details). We also give at 1.1 GeV the total cross section obtained with  $C_5^A(0) = 1.2$ . Right: QE and full model predicted antineutrino CC inclusive cross section per nucleon, as a function of the antineutrino energy.

RPA and other nuclear effects, which importance diminishes when the transferred energy increases.

To end this section in Fig. 19 we show total and QE inclusive cross sections for both neutrino and antineutrino modes. In the neutrino case, we compare our results with the recent data published by the SciBooNE collaboration. We display SciBooNE data-sets based on NEUT and NUANCE Monte Carlo event generators. We find a reasonable description, taking into account experimental and theoretical uncertainties, up to neutrino energies around 1 GeV. At larger energies, we underestimate the cross section, as anticipated above. For instance, we see how some 2p2h1 $\pi$  contributions neglected in our model, become relatively important at  $E_\nu = 1$  GeV. More specifically, the empty circle is obtained when the  $\Delta$ -resonance contribution to the imaginary part of  $U$  is kept in the evaluation of the imaginary part of the  $\pi$ - and  $\rho$ -selfenergies in Eqs. (29) and (44). There are some other  $W^+NN \rightarrow NN\pi$  mechanisms which should be taken into account, as well as the contribution of higher resonances [58]. Though small, also kaon [59], hyperon [60] and two pion [61] production channels should be considered to end up with a robust theoretical model above 1 GeV.

#### IV. CONCLUSIONS

We have developed a model for the study of weak CC induced nuclear reactions at intermediate energies of interest for current and future neutrino oscillation experiments. This model is an extension of the work of Ref. [2] that analyzed the QE contribution to the inclusive neutrino scattering on nuclei. The model is based on a systematic many body expansion of the gauge boson absorption modes that includes one, two and even three body mechanisms, as well as the excitation of  $\Delta$  isobars. The whole scheme has no free parameters, besides those previously adjusted to the weak pion production off the nucleon cross sections in the deuteron, since all nuclear effects were set up in previous studies of photon, electron and pion interactions with nuclei.

We have discussed at length the recent CCQE MiniBooNE cross section data. To understand these measurements, it turns out to be essential the consideration of mechanisms where the  $W$ -boson is absorbed by two or more nucleons without producing pions, as first suggested by M. Martini and collaborators [27]. Our evaluation of these pionless multinucleon emission contributions to the cross section is fully microscopical and it contains terms, which were either not considered or only approximately taken into account in [27]. We end up with a reasonable description of the neutrino CC"QE" MiniBooNE and total inclusive SciBooNE cross section data up to neutrino energies of around 1 GeV.

Our results do not support the incompatibility among neutrino and electron-nucleus inclusive data claimed in [22], since our neutrino model is just a natural extension of that developed in Refs. [1] and [37] to study electron- and photo-nuclear inclusive reactions. Indeed, we believe that the origin of the problem can be traced back to the difficulties of the spectral function model advocated in [22] to properly describe the *dip* and  $\Delta$ - regions for electron

scattering, together with the mismatch existing in the definition of the quasielastic contribution between the theory and the experimental neutrino communities.

The recent CC MiniBooNE and SciBooNE inclusive data sets provide very valuable information to distinguish among different models. This will definitely help to unravel the details about the modification of the CC weak current properties inside of the nucleus, and will set up the basis to construct a robust theoretical framework where all electroweak nuclear reactions at intermediate energies could be studied. This is in turn of special relevance to better understand the systematic errors affecting present (MiniBooNE & T2K) and coming neutrino oscillation experiments involving neutrinos with energies below 1 GeV. Future antineutrino data, similar to the CCQE MiniBooNE measurements of total and differential neutrino cross sections, will further constraint any theory.

We think the microscopical model presented here, which extends that of Ref. [2] beyond the QE region, constitutes a first step towards this goal. The model should be extended still to higher energies, which would make possible the comparison of its predictions to the MiniBooNE differential cross section data. This is a non trivial task, but it will allow for a better knowledge of the axial currents both for hadrons and nuclei.

### Acknowledgments

This research was supported by DGI and FEDER funds, under contracts FIS2008-01143/FIS, FIS2006-03438, and the Spanish Consolider-Ingenio 2010 Programme CPAN (CSD2007-00042), by Generalitat Valenciana contract PROMETEO/2009/0090 and by the EU HadronPhysics2 project, grant agreement n. 227431. I.R.S. acknowledges support from the Ministerio de Educación.

- 
- [1] A. Gil, J. Nieves and E. Oset, Nucl. Phys. A **627** (1997) 543.
  - [2] J. Nieves, J. E. Amaro and M. Valverde, Phys. Rev. C **70** (2004) 055503 [Erratum-ibid. C **72** (2005) 019902].
  - [3] A. A. Aguilar-Arevalo *et al.* [MiniBooNE Collaboration], Phys. Rev. D **81** (2010) 092005.
  - [4] A. A. Aguilar-Arevalo *et al.* [MiniBooNE Collaboration], Phys. Rev. D **82** (2010) 092005.
  - [5] A. A. Aguilar-Arevalo *et al.* [MiniBooNE Collaboration], arXiv:1011.3572 [hep-ex].
  - [6] Y. Nakajima *et al.* [SciBooNE Collaboration], Phys. Rev. D **83** (2011) 012005.
  - [7] L. Alvarez-Ruso, arXiv:1012.3871 [nucl-th].
  - [8] O. Benhar, N. Farina, H. Nakamura, M. Sakuda, R. Seki, Phys. Rev. **D72** (2005) 053005.
  - [9] A. M. Ankowski, J. T. Sobczyk, Phys. Rev. **C77** (2008) 044311.
  - [10] A. M. Ankowski, O. Benhar, N. Farina, Phys. Rev. **D82** (2010) 013002.
  - [11] C. Maieron, M. C. Martinez, J. A. Caballero, J. M. Udias, Phys. Rev. **C68** (2003) 048501.
  - [12] M. C. Martinez, P. Lava, N. Jachowicz, J. Ryckebusch, K. Vantournhout and J. M. Udias, Phys. Rev. C **73** (2006) 024607.
  - [13] T. Leitner, O. Buss, L. Alvarez-Ruso and U. Mosel, Phys. Rev. C **79** (2009) 034601
  - [14] J. Nieves, M. Valverde and M. J. Vicente Vacas, Phys. Rev. C **73** (2006) 025504.
  - [15] S. K. Singh, E. Oset, Nucl. Phys. **A542** (1992) 587–615.
  - [16] M. Sajjad Athar, S. Chauhan, S. K. Singh, Eur. Phys. J. C **A43** (2010) 209–227.
  - [17] A. Bodek, S. Avvakumov, R. Bradford and H. S. Budd, Eur. Phys. J. C **53** (2008) 349.
  - [18] A. Liesenfeld *et al.* [A1 Collaboration], Phys. Lett. B **468** (1999) 20.
  - [19] V. Bernard, N. Kaiser and U. G. Meissner, Phys. Rev. Lett. **69** (1992) 1877.
  - [20] S. Boyd, S. Dytman, E. Hernandez, J. Sobczyk, R. Tacik, AIP Conf. Proc. 1189 (2009) 60–73.
  - [21] A. V. Butkevich, Phys. Rev. C **82** (2010) 055501.
  - [22] O. Benhar, P. Coletti, D. Meloni, Phys. Rev. Lett. **105** (2010) 132301.
  - [23] C. Juszczak, J. T. Sobczyk and J. Zmuda, Phys. Rev. C **82** (2010) 045502.
  - [24] V. Lyubushkin *et al.* [NOMAD Collaboration], Eur. Phys. J. C **63** (2009) 355.
  - [25] J. E. Amaro, M. B. Barbaro, J. A. Caballero, T. W. Donnelly and C. F. Williamson, Phys. Lett. B **696**, 151 (2011).
  - [26] J. E. Amaro, M. B. Barbaro, J. A. Caballero and T. W. Donnelly, arXiv:1012.4265.
  - [27] M. Martini, M. Ericson, G. Chanfray, J. Marteau, Phys. Rev. **C80** (2009) 065501.
  - [28] M. Martini, M. Ericson, G. Chanfray, J. Marteau, Phys. Rev. **C81** (2010) 045502.
  - [29] L. Alvarez-Ruso, S. K. Singh, M. J. Vicente Vacas, Phys. Rev. **C59** (1999) 3386–3392.
  - [30] T. Sato, D. Uno, T. S. H. Lee, Phys. Rev. **C67** (2003) 065201.
  - [31] K. M. Graczyk, D. Kielczewska, P. Przewlocki, J. T. Sobczyk, Phys. Rev. **D80** (2009) 093001.
  - [32] E. Hernandez, J. Nieves and M. Valverde, Phys. Rev. D **76** (2007) 033005.
  - [33] T. Leitner, O. Buss, U. Mosel and L. Alvarez-Ruso, Phys. Rev. C **79** (2009) 038501.
  - [34] T. Leitner and U. Mosel, Phys. Rev. C **82** (2010) 035503
  - [35] E. Hernandez, J. Nieves, M. Valverde and M. J. Vicente Vacas, Phys. Rev. D **81** (2010) 085046.
  - [36] O. Lalakulich, T. Leitner, O. Buss and U. Mosel, Phys. Rev. D **82** (2010) 093001



- [37] R. C. Carrasco and E. Oset, Nucl. Phys. A **536** (1992) 445.
- [38] E. Oset, H. Toki and W. Weise, Phys. Rept. **83** (1982) 281.
- [39] L. L. Salcedo, E. Oset, M. J. Vicente-Vacas and C. Garcia-Recio, Nucl. Phys. A **484** (1988) 557.
- [40] J. Nieves, E. Oset and C. Garcia-Recio, Nucl. Phys. A **554** (1993) 509.
- [41] J. Nieves, E. Oset and C. Garcia-Recio, Nucl. Phys. A **554** (1993) 554.
- [42] C. Albertus, J. E. Amaro and J. Nieves, Phys. Rev. Lett. **89** (2002) 032501.
- [43] M. Valverde, J. E. Amaro and J. Nieves, Phys. Lett. B **638** (2006) 325.
- [44] J. E. Amaro, C. Maieron, J. Nieves and M. Valverde, Eur. Phys. J. A **24** (2005) 343 [Erratum-ibid. A **26** (2005) 307].
- [45] J. E. Amaro, A. M. Lallena and J. Nieves, Nucl. Phys. A **623** (1997) 529.
- [46] D. Drechsel, S. S. Kamalov and L. Tiator, Eur. Phys. J. A **34**, 69 (2007).
- [47] C. Garcia-Recio, E. Oset and L. L. Salcedo, Phys. Rev. C **37** (1988) 194.
- [48] E. Oset and L. L. Salcedo, Nucl. Phys. A **468** (1987) 631.
- [49] P. Fernandez de Cordoba and E. Oset, Phys. Rev. C **46** (1992) 1697.
- [50] M. Benmerrouche, R. M. Davidson and N. C. Mukhopadhyay, Phys. Rev. C **39** (1989) 2339.
- [51] M. Hirata, J. H. Koch, E. J. Moniz and F. Lenz, Annals Phys. **120** (1979) 205.
- [52] L. Alvarez-Ruso, L. S. Geng, S. Hirenzaki and M. J. Vicente Vacas, Phys. Rev. C **75** (2007) 055501 [Erratum-ibid. C **80** (2009) 019906].
- [53] J. E. Amaro, E. Hernandez, J. Nieves and M. Valverde, Phys. Rev. D **79** (2009) 013002; E. Hernandez, J. Nieves and M. Valverde, Phys. Rev. D **82** (2010) 077303
- [54] L. Alvarez-Ruso, L. S. Geng and M. J. Vicente Vacas, Phys. Rev. C **76** (2007) 068501 [Erratum-ibid. C **80** (2009) 029904].
- [55] T. Leitner and U. Mosel, Phys. Rev. C **81**, 064614 (2010).
- [56] L. B. Auerbach *et al.* [ LSND Collaboration ], Phys. Rev. **C66** (2002) 015501.
- [57] O. Benhar and D. Meloni, Phys. Rev. D **80** (2009) 073003.
- [58] O. Lalakulich, E. A. Paschos and G. Piranishvili, Phys. Rev. D **74** (2006) 014009.
- [59] M. Rafi Alam, I. Ruiz Simo, M. Sajjad Athar and M. J. Vicente Vacas, Phys. Rev. D **82** (2010) 033001.
- [60] S. K. Singh and M. J. Vicente Vacas, Phys. Rev. D **74** (2006) 053009.
- [61] E. Hernandez, J. Nieves, S. K. Singh, M. Valverde and M. J. Vicente Vacas, Phys. Rev. D **77** (2008) 053009.